

# Shear Strength of Reinforced Mortar Beams Containing Polyvinyl Alcohol Fibre (PVA)

Mohamed Said<sup>1</sup> · Wael Montaser<sup>2</sup> · Ahmed S. Elgammal<sup>2</sup> · Amr H. Zahir<sup>3</sup> · Ibrahim G. Shaaban<sup>4</sup> 

## Abstract

The current study aims to assess the shear behaviour of reinforced mortar beams including Polyvinyl Alcohol Fibre (PVA) ranges from 0 to 2.25%, fly ash (55%) and silica fume (15%). Fourteen beams were experimentally tested under two concentrated loads. In addition, a finite element model was developed to predict the crack pattern, load–deflection, energy absorption, and shear strength results of the test beams. The studied variables were different percentages of PVA fibres, shear span to depth ratio ( $a/d$ ), and transverse reinforcement (stirrups) ratio. The fly ash and silica fume were kept constant in all the studied mixes to achieve a compressive strength above 55 MPa at the time of testing (90 days) and to improve PVA-mortar properties. It was found that the inclusion of PVA improves the shear behavior of the tested beams in terms of crack pattern and ductility. It was observed also that reducing  $a/d$  led to enhancing the shear capacity without changing the mode of failure. In addition, PVA played the same role as the stirrups and their effect on the ultimate shear capacity was increased with reducing the volume of stirrups. Moreover, the PVA fibres were more effective in lower shear span to depth ratio ( $a/d = 1.5$ ) giving an enhancement of shear resistance of 221%. The non-linear finite element model showed excellent agreement with the experimental results and the ratio of the predicted to experimental ultimate strength ranged between 0.91 and 1.09. The authors recommend a combination of fly ash, silica fume and at least 1.5% PVA in the presence of minimum stirrups reinforcement ( $5\Phi 6/m$ ) or adding 2.25% PVA without stirrups to achieve adequate shear behaviour and to improve the ductility of PVA-mortar beams.

**Keywords** PVA · Mortar · Shear of beams · Fly ash · Silica fume · Non-linear finite element modeling

✉ Ibrahim G. Shaaban  
ibrahim.shaaban@uwl.ac.uk

Mohamed Said  
mohamed.abdelghaffar@feng.bu.edu.eg

Wael Montaser  
wmontaser.eng@o6u.edu.eg

Ahmed S. Elgammal  
eng.a.sherif93@gmail.com

Amr H. Zahir  
amr\_h\_zaher@yahoo.com

<sup>1</sup> Civil Engineering Department, Faculty of Engineering (Shoubra), Benha University, Banha, Egypt

<sup>2</sup> Construction and Building Department, Faculty of Engineering, October 6 University, Al Mehwar Al Markazi, Egypt

<sup>3</sup> Structural Engineering Department, Faculty of Engineering, Ain Shams University, Cairo, Egypt

<sup>4</sup> School of Computing and Engineering, University of West London, London, UK

## 1 Introduction

Polyvinyl Alcohol fibre (PVA) is an environment friendly fibre with excellent alkali resistance. PVA fibre is economic, exhibits higher tensile strength and elastic modulus compared to polypropylene (PP) fibre [1]. Researchers [1–4] reported that the overall cost of mortar/concrete composites including PVA, such as Engineered Cementitious Composites (ECC), can be reduced by using an optimized dosage of micro-fibres and local materials including cement, fine aggregate, cement replacement materials such as fly ash and silica fume, and chemical admixtures. Iqbal Khan et al. [4] reported that the use of coarse aggregates increased the fibre balling, which reduced the micro-fibre dispersion effectiveness. Therefore, researchers [5, 6] eliminated the coarse aggregates in their mixes and only smaller amount of fine sand was used to control fracture toughness of matrix for PVA-mortar

24  
25

26  
27  
28  
29  
30  
31  
32  
33  
34  
35  
36  
37  
38  
39  
40  
41

42	composite production. Zhu et al. [7] reported the benefit of	[7, 14, 15], because the pozzolanic reaction of silica fume	95
43	adding silica fume and fly ash in improving durability and	and fly ash takes place after the initial hydration of cement	96
44	compressive strength of PVA-mortar composite elements.	and continues to 90 days and beyond [12, 15].	97
45	Kanda et al. [8], used PVA fibres to produce ECC and they	In the above reviewed literature, the importance of PVA	98
46	reported that the PVA is the main contributor to achieve the	fibres in improving the ductility of composite mortar was	99
47	high strain hardening and ductility for ECC. Furthermore,	reported. The negative effect of coarse aggregate on the	100
48	Kanda et al. [9] described the design concept and material	efficiency of PVA fibres was addressed. The positive effect	101
49	characteristics of PVA composite mortar elements. They	of PVA with fly ash on the shear behaviour of mortar	102
50	showed that composites containing PVA exhibited a	beams was mentioned. The improvement of PVA-mortar	103
51	remarkably ductile tensile property with more than 1%	composite elements durability by adding silica fume	104
52	tensile strain capacity, which in turn, has enhanced struc-	(5–15%) and fly ash (50–65%) with PVA fibres was also	105
53	tural performance in seismic conditions.	reported.	106
54	Alyousif et al. [10] studied the shear behaviour of PVA-	<b>2 Research Significance</b>	107
55	mortar beams cast with fly ash and different shear span	Based on the research gap from the above literature review,	108
56	lengths. The test results showed that the behaviour of these	the current study aims to investigate the shear behaviour of	109
57	beams under shear was, in most cases, much better than	PVA-reinforced mortar beams containing a fixed content of	110
58	that of conventional reinforced concrete beams without	fly ash (55%) and silica fume (15%), as recommended in	111
59	PVA. The strength, stiffness, ductility and energy absorp-	the literature, and different percentages of PVA up to	112
60	tion capacity of mortar beams with PVA were found to be	2.25%. The research focuses on the effect of PVA in the	113
61	significantly higher than those of the corresponding rein-	presence of silica fume and fly ash after curing for 90 days	114
62	forced concrete beams without PVA, to varying degrees,	on the structural behaviour and shear strength of studied	115
63	based on the shear span to depth ratio. Paegle et al. [11]	beams. This will be achieved by testing 17 mortar beams	116
64	also studied the shear behaviour of PVA-mortar beams.	containing different percentages of PVA with and without	117
65	Their experimental program consisted of reinforced mortar	stirrups. Finite element modeling of the test beams was	118
66	beams with short (8 mm) randomly distributed PVA fibre	carried out using ANSYS to predict the crack pattern, load-	119
67	and conventional reinforced concrete counterparts for	deflection, and shear capacity results.	120
68	comparison with varying shear reinforcement arrange-	<b>3 Experimental Program</b>	121
69	ments. The results demonstrated that the PVA-mortar	<b>3.1 Constituent Materials</b>	122
70	beams had better shear resistance, better control of crack	The mix ingredients used throughout this investigation	123
71	sizes, and a more ductile shear failure compared to the	were Portland cement, fly ash, silica fume, polyvinyl	124
72	conventional reinforced concrete beams. Liu et al. [12]	alcohol (PVA) micro-fibres, natural siliceous sand, water,	125
73	reported that adding high content of fly ash (67%) to PVA-	high range water reducer (HRWR), and reinforcing steel.	126
74	mortar composites resulted in self-healing of micro-cracks	The properties of these materials are given in the following	127
75	in structural elements under sulfate and chloride attack.	sections.	128
76	Ismail et al. [13] studied the shear behaviour of large-	<b>3.1.1 Cement and Cement Replacement Materials</b>	129
77	scale composite beams reinforced with different types of	A grade 52.5 Portland cement was supplied by a local	130
78	PVA and steel fibres (PVA8, PVA12, PP19, and long steel	Egyptian factory, and is compatible with European stan-	131
79	fibres, SF13). Their beams showed better performance in	dards [16]. Type F fly ash was obtained from CEMEN-	132
80	terms of cracking behaviour, shear capacity, ductility and	TRAC Company for Cement Exporting. Fly ash complied	133
81	energy absorption compared with normal reinforced con-	with ASTM C 618 [17]. The silica fume was supplied by	134
82	crete beams. Beams reinforced with PVA-8 fibres showed	Sika Egypt for Construction Chemicals and it was com-	135
83	the highest shear strength and ductility compared to the	plied with ASTM C 1240 [18]. The physical and chemical	136
84	beams containing other polymeric fibres. Longer PVA	properties of cement replacement materials are shown in	137
85	fibres appeared to be less efficient than shorter ones. The	Tables 1 and 2 (provided by the supplier). In addition, the	138
86	beam reinforced with PP19 showed the lowest perfor-		
87	mance, while the use of SF13 proved to be the most		
88	effective in improving the first crack load, ultimate load,		
89	ductility and energy absorption capacity. The researchers		
90	reported that the fly ash range (50–65%) and silica fume		
91	(5–15%) were the best combination for improving		
92	mechanical properties and durability aspects of PVA-		
93	mortar/concrete elements. This improvement was optimum		
94	when testing was conducted at the age of 90 days		

139 physical and chemical properties of cement is presented in  
140 Table 3.

### 141 3.1.2 Polyvinyl Alcohol Fibre (PVA)

142 Different volume percentages of polyvinyl alcohol (PVA)  
143 fibres (0.75, 1.5, and 2.25%) were used in the mortar  
144 beams. The properties of PVA fibre are listed in Table 4  
145 (provided by the supplier). The same mechanical properties  
146 PVA fibres were presented by Cao [19] and Said et al. [20]

### 147 3.1.3 Sand

148 Fine aggregate, used in sample preparation, was natural  
149 siliceous sand. The fine aggregate was clean, free of  
150 impurities and with no organic compounds with fineness  
151 modulus 2.84. Sieve analysis test was carried out in  
152 accordance with the ESS No. 1109/2002 [21] and the test  
153 results are shown in Table 5. Moreover, the sieve analysis  
154 curve of the fine aggregate is presented in Fig. 1.

### 155 3.1.4 Water and High Range Water Reducer

156 Potable tap water is used for mixing and curing of the test  
157 specimens. Polycarboxylic High Range Water Reducer  
158 (HRWR) from BASF Construction Chemicals (Master  
159 Glenium RMC 315) complying with BS EN 934-2 [22] was  
160 used. The objective of adding HRWR was to ensure that  
161 the PVA fibres were well-dispersed in the mixes and to  
162 achieve workability as indicated by a slump of  
163 60 mm  $\pm$  10 mm.

### 164 3.1.5 Reinforcing Steel

165 The longitudinal reinforcement for the beams was high  
166 tensile steel (40/60) having 450 MPa yield stress. Mild  
167 steel (24/35) having 240 MPa yield stress was used for  
168 stirrups. The size of bars used for longitudinal

**Table 1** Properties of the used silica fume

SiO <sub>2</sub>	> 88.9%
Moisture	< 0.57%
Alkalis like Na <sub>2</sub> O	< 0.5%
Free CaO	< 0.1%
Free SI	0.14%
Free Cl%	0.02%
SO <sub>3</sub>	< 0.25%
L.O.I (incl. carbon)	< 4.5%
Specific surface	~ 20 m <sup>2</sup> /g
Size	~ 0.15 microns

**Table 2** Properties of the used fly ash

Density (Kg/m <sup>3</sup> )	2150
Activity index % (after 28 days)	77.5
Activity index % (after 90 days)	85.6
Soundness (mm)	1
Fineness %	22.43
LOI %	3.82
SiO <sub>2</sub> %	57.87
Al <sub>2</sub> O <sub>3</sub> %	26.12
Fe <sub>2</sub> O <sub>3</sub> %	5.68
CaO%	1.163
SO <sub>3</sub> %	< 0.00010
Alkalis%	2.46
Free CaO	0.03
Cl %	< 0.00020
Reactive SiO <sub>2</sub> %	40.34
Blaine (cm <sup>2</sup> /g)	3330

**Table 3** Physical and mechanical properties of cement

Property	Measured value
Fineness (mm <sup>2</sup> /N)	3260
Specific gravity	3.15
Soundness (expansion, %)	0.50
Initial setting time (min.)	75'
Final setting time (min.)	180'
Crushing strength (MPa)	
3 days	23.9
7 days	26.52
28 days	35
Silica dioxide (SiO <sub>2</sub> ) %	21.45%
Aluminum oxide (Al <sub>2</sub> O <sub>3</sub> ) %	5.80%
Iron oxide (Fe <sub>2</sub> O <sub>3</sub> ) %	3.60%
Calcium oxide (CaO) %	63.63%
Magnesium oxide (MgO) %	1.4%
Sulphur trioxide (SO <sub>3</sub> ) %	3.17%
Moisture %	-
Loss due to ignition %	4.10%

169 reinforcement was 18 mm diameter and for the stirrups, it  
170 was 6 mm diameter. The steel reinforcement properties  
171 were according to [23, 24].

**Table 4** Properties of the polyvinyl alcohol fibres (PVA)

Length ( $l_f$ ) (mm)	Shape	Diameter ( $\phi_f$ ) (mm)	Tensile strength (MPa)	Elastic modulus (GPa)	Density ( $\rho$ ) (g/ cm <sup>3</sup> )	Elongation (%)
12	Monofilament	0.04	1620	42.80	1.3	7.0

### 3.2 Mixing Process, Specimen Preparation, and Curing

Trial mixes were carried out varying the percentage of water binder ratio ( $w/b$ ) to obtain the required  $f_{cu}$  ( $> 55$  MPa at 90 days). Finally, the ( $w/b$ ) ratio and sand to binder ratio were kept constant for all mixes at 0.33 and 0.8, respectively. The fly ash content was 55% and silica fume content was 15% of the total binder (Portland cement + fly ash + silica fume) as recommended in literature. HRWR was added with dosage ranges from 0.9 to 1.25% by weight of binder. The final quantities required by weight for one cubic meter of fresh concrete for the specimens are given in Table 6. The mixing process was according to the method described by Zhou et al. [25] to achieve good fibre dispersion. At the final stage of mixing, all materials were mechanically mixed in a drum mixer for 2 min and cast in the wooden forms, in which the reinforcing steel cages were previously placed. The poured PVA-mortar was then vibrated with an electrical Poker vibrator and the final surface was smoothed using a trowel. The forms were removed after 24 h from casting and specimens were kept under wet burlap, sprayed with water twice a day for 28 days and then kept in laboratory atmosphere for 90 days until they were tested.

To test the mechanical properties of the PVA-mortar composite, companion samples from the same mixes were prepared during casting the beam specimens. These

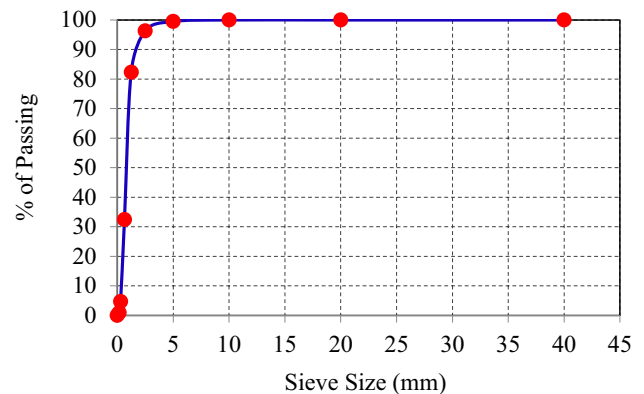
samples were de-moulded 24 h after casting and were continuously water cured for 28 days (except for the cube samples that were tested for compressive strength at 7 days). Thereafter, these samples were kept in the laboratory near their corresponding beam samples until their testing age (i.e. some cubes were tested for compressive strength at 28 and 56 days, whilst the remainder of the samples were tested at 90 days).

### 3.3 Details of Test Specimens

The experimental program comprised 14 large-scale beams of span ( $L$ ) = 1800 mm, depth ( $t_b$ ) = 300 mm, and width ( $b$ ) = 120 mm. The effective depth for all specimens was 260 mm. The beams were simply supported and tested under the effect of four-point bending. The main four variables were the volume of the PVA fibres (0, 0.75%, 1.5%, 2.25%), variable shear span-to-depth ratio,  $a/d$  (2.25, 1.5) and variable distribution of stirrups (5 $\Phi$ 6/m, 7.5 $\Phi$ 6/m, 10 $\Phi$ 6/m). The test beams represented four Groups A, B, C, D, and E as indicated in Table 7. All beams were designed according to ECP 203–2007 [24] to be very strong in flexure and very weak in shear to assess the PVA fibre effect on shear behaviour. The steel bars were tied with the stirrups forming reinforcement cages as shown in Fig. 2. Electrical strain gauges of 10 mms length and  $120.3 \pm 0.5$ - $\Omega$  resistance were fixed on the steel bars, with the positions shown in Fig. 3 to follow the reinforcement strains during loading. The strain gauges were covered with silicon sealant to protect them during casting and consolidation of concrete.

**Table 5** Sieve analysis test results for fine aggregates

Sieve size (mm)	Retained on each size (gm.)	Cumulative retained	Cumulative retained %	Passing %
40	0	0	0	100
20	0	0	0	100
10	0	0	0	100
5	5	5	0.5	99.5
2.5	32	37	3.7	96.3
1.25	140	177	17.7	82.3
0.65	496	673	67.6	32.4
0.3	280	953	95.3	4.7
0.16	38	991	99.1	0.9
Pan	9	1000	100	0

**Fig. 1** Sieve analysis curve of the fine aggregate

**Table 6** Mix proportions for mortars (Kg/m<sup>3</sup>)

Mix	Cement	Fly ash (55%)	Silica fume (15%)	Fine sand	Water	PVA Fibres		HRWR
						(Kg)	%	
1	360	660	180	960	400	0	0.0	11
2	360	660	180	960	400	10	0.75	11
3	360	660	180	960	400	20	1.50	13
4	360	660	180	960	400	33	2.25	15

228 The mechanical property specimens consisted of twelve  
 229 cube specimens (100 mm each side) from each mix to test  
 230 the compressive strength at different ages (three cubes  
 231 from each mix were tested at 7, 28, 56 and 90 days). In  
 232 addition, three cylindrical specimens (100 diameter and  
 233 200 mm height) for prepared from each mix to test the  
 234 splitting tensile strength at 90 days. Moreover, three  
 235 cylindrical specimens were prepared to obtain compressive  
 236 stress-strain relationships per mix, and to calculate the  
 237 Young's modulus at the age of 90 days. Therefore, six  
 238 cylinders were prepared from each mix.

**Table 7** Details of the tested beams

Group	Beam	Shear span to depth ratio ( <i>a/d</i> )	PVA, <i>V<sub>f</sub></i> %	Stirrups	Mix
A	B1	2.5	0.00	–	1
	B2		0.75	–	2
	B3		1.50	–	3
	B4		2.25	–	4
B	B5	1.5	0.00	–	1
	B6		0.75	–	2
	B7		1.50	–	3
	B8		2.25	–	4
C	B9	2.25	1.50	5Φ6/m	3
	B10		1.50	7.5 Φ 6/m	3
	B11	2.25	1.50	10 Φ 6/m	3
d	12		0.75	5 Φ 6/m	2
	13		0.75	7.5 Φ 6/m	2
	14		0.75	10 Φ 6/m	2
e	15	2.25	0.00	5 Φ 6/m	1
	16		0.00	7.5 Φ 6/m	1
	17		0.00	10 Φ 6/m	1

### 3.4 Testing of Specimens

239  
 240 At the day of testing, the beam specimen was mounted and  
 241 adjusted in the loading frame. The beams were loaded in  
 242 increments up to failure. They were instrumented to mea-  
 243 sure their deformational behavior after each load incre-  
 244 ment. Test setup is shown in Fig. 4. The recorded  
 245 measurements include concrete, longitudinal reinforcement  
 246 and stirrups strain, lateral deflection and crack propagation.  
 247 The reinforcement strains were measured using the elec-  
 248 trical strain gauges (extensometer) of 10 mm gauge length  
 249 attached to longitudinal reinforcement and stirrups as  
 250 shown in Fig. 3. The electrical strain gauges were coupled  
 251 to a strain indicator. The deflections were measured using  
 252 three Linear Variable Displacement Transducers (LVDT)  
 253 100 mm capacity and 0.01 mm accuracy and arranged to  
 254 measure the deflection distribution to the specimen as  
 255 shown in Fig. 3. After each load increment, the cracks were  
 256 traced and marked on the painted sides of the specimen  
 257 according to their priority of occurrence.

**Fig. 2** Steel reinforcement cages for typical specimens

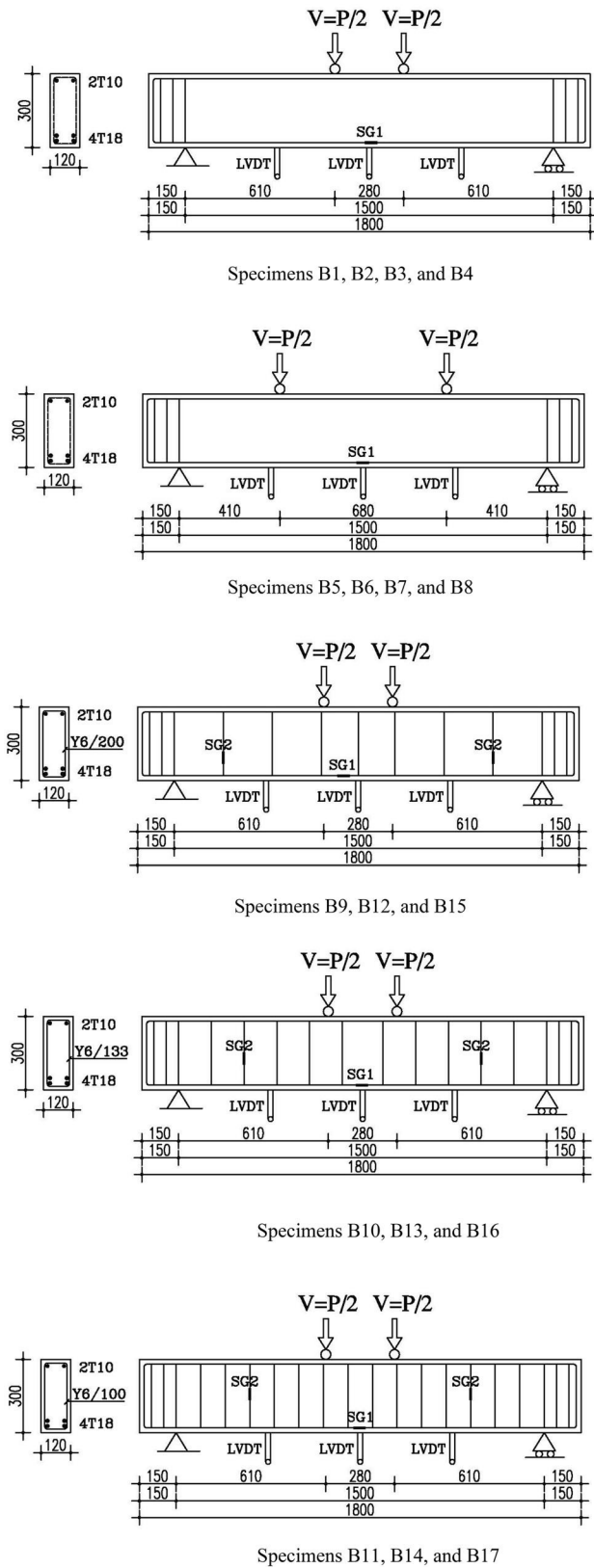


**Fig. 3** Position of demec points, electrical strain gauges, and LVDTs



**Fig. 4** Test setup for a typical beam

The tests for the mechanical properties of the samples were conducted using a 2000 KN capacity universal testing machine. The compressive and indirect tensile samples were tested to failure. Tests for the stress–strain relationship and Young’s modulus were under deformation control with a displacement rate of 0.05 mm/min, in which cylinders were loaded up to 40% of the expected ultimate load. Details of the mechanical testing properties are reported elsewhere [26].

## 4 Experimental Results and Discussion

### 4.1 Mechanical Properties for Test Specimens

Table 8 shows the average values (from the three samples tested for each mix) of the mechanical properties for the PVA-mortar mixes. The experimental stress–strain curves for the mixes are presented in Fig. 5. It can be seen from Table 8 that the compressive strength and Young’s modulus values were similar for all the mixes. However, the

**Table 8** Average test results of compressive, splitting tensile strength, and Young’s modulus

Mix	Compressive strength (MPa)				Splitting tensile strength (MPa) at 90 days	Young’s Modulus (GPa) at 90 days
	7 days	28 days	56 days	90 days		
1	24	44	49	58	5.9	17.3
2	26	45	48	58	8.0	17.8
3	25	44	47	57	10.0	17.6
4	23	43	46	55	13.0	17.5

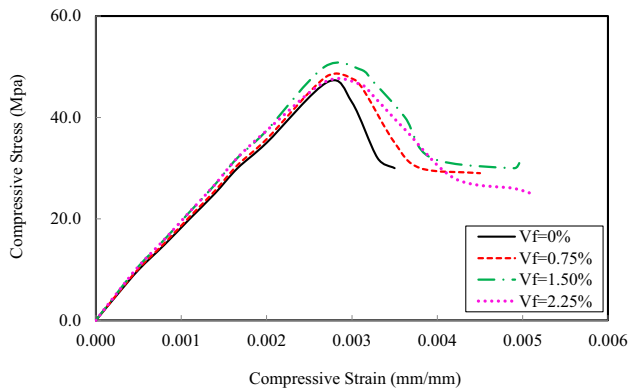


Fig. 5 Compressive stress–strain curves of the mixes

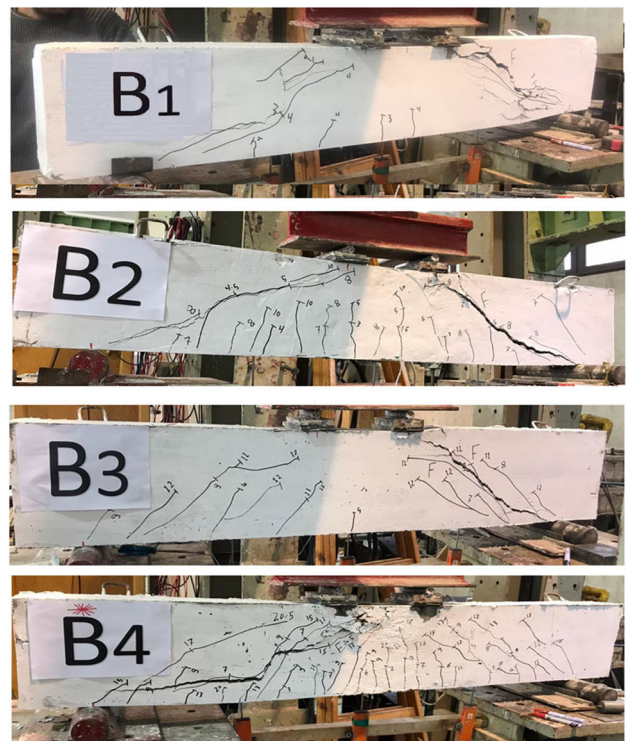
275 effect of PVA on splitting tensile strength was highly  
 276 significant, increasing with the increase of PVA content in  
 277 the mix. For example, the specimens of  $V_f = 2.25\%$ ,  $1.5\%$ ,  
 278  $0.75\%$  were higher than that of mortar specimens with no  
 279 PVA by 160%, 100%, and 60%, respectively. The stress–  
 280 strain curves in Fig. 5, also show a similar trend as the  
 281 maximum compressive strength on the curves was only  
 282 slightly affected by PVA content (ranging between 46 and  
 283 49.5 MPa for all mixes), but the ductility increased with  
 284 increasing the percentage of PVA. This can be indicated by  
 285 a higher strain at failure, i.e. higher maximum strain, and  
 286 larger area under the stress–strain curves as seen in Fig. 9.  
 287 Samples with 2.25%, 1.5%, 0.75% and 0% PVA, had  
 288 ultimate strains of 0.0051, 0.0049, 0.0045 and 0.0035,  
 289 respectively. Hence, the maximum strain of specimens of  
 290  $V_f = 2.25\%$ ,  $1.5\%$ ,  $0.75\%$  were higher than that of mortar  
 291 specimens with no PVA by 46%, 40%, and 29%, respec-  
 292 tively. The order of magnitude of the values agrees with the  
 293 results of Meng et al. [26] who reported that the average  
 294 cylinder compressive strength results of nine PVA-mortar  
 295 cylinders was 48.4 MPa and corresponding strains were in  
 296 the order of 0.0055, whereas the average Young’s modulus  
 297 of the PVA-mortar samples was 18.1 GPa.

## 4.2 Crack Patterns and Failure Mode

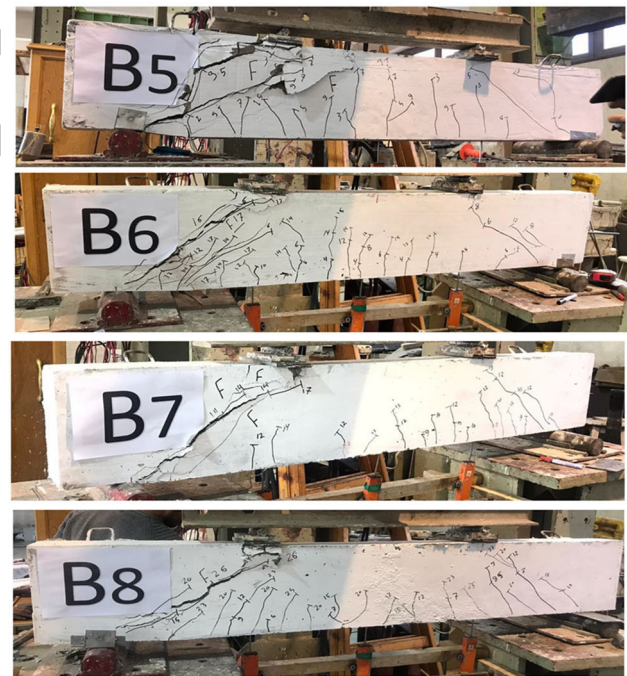
298  
 299 All cracks were outlined and labelled at each loading stage  
 300 with a black marker and crack width was measured using  
 301 crack measuring scale. Figure 6a–e show the crack pattern  
 302 and failure modes of all the test beams while the first  
 303 flexural crack, shear crack, ultimate loads, deflections, and  
 304 energy absorption which representing ductility are recorded  
 305 in Table 9.

### 4.2.1 Group A

306  
 307 Crack pattern and failure modes of beams comprising  
 308 Group A of  $a/d$  equals 2.25, and no stirrups, B1, B2, B3,



(a) Group A

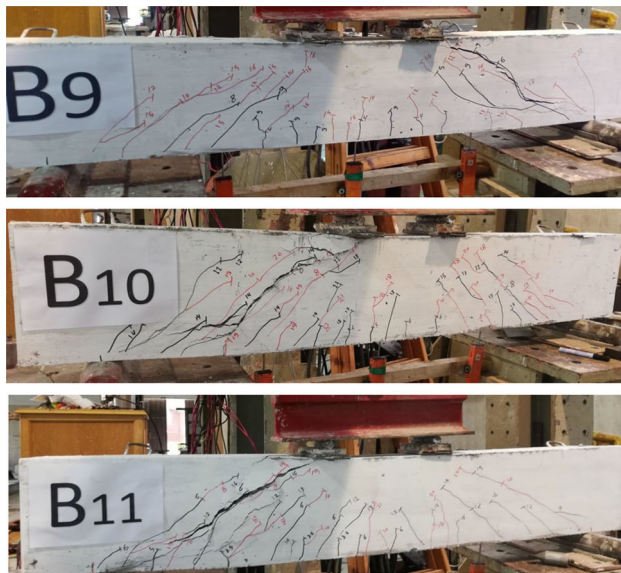


(b) Group B

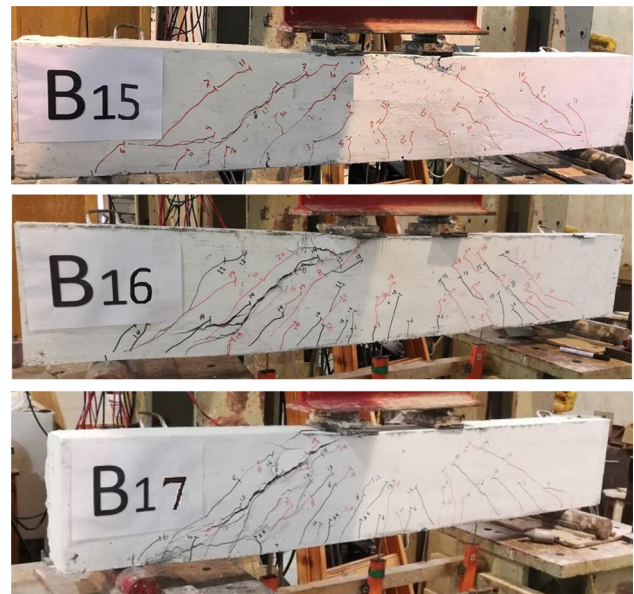
Fig. 6 Crack patterns and failure modes of experimentally tested beams

and B4 are shown in Fig. 6a. It can be seen from the figure and Table 9 that B1, with no PVA fibres, had the first flexural cracking load at 22 kN, then shear cracks started at

309  
 310  
 311



(c) Group C



(e) Group E



(d) Group D

Fig. 6 continued

312 27 kN, and the beam failure was brittle in a large diagonal  
 313 shear crack at ultimate load of 89.5 kN. For B2 including  
 314 0.75% PVA, the first flexural crack started at 32 kN, the  
 315 shear cracks started at 38 kN, and the failure was in a large  
 316 diagonal shear crack at 134 kN. Increasing the PVA% to  
 317 1.5 for B3, led to raising the first flexural cracking load to  
 318 40 kN with more flexural cracks as warnings, the shear  
 319 loads raised to 50 kN, and the failure was also shear at  
 320 higher ultimate load, 170 kN. A further increase of the  
 321 PVA% to 2.25% led to a higher first crack load, 48 kN,  
 322 higher shear crack load, 60 kN, and the failure was due to

Fig. 6 continued

diagonal shear at 203.3 kN after several warnings of many  
 323 flexural cracks indicating the ductile behaviour of the beam  
 324 as can be observed from the increase in the energy  
 325 absorption.  
 326

#### 4.2.2 Group B

327  
 328 Group B specimens of  $a/d$  equals 1.5, and no stirrups, B5,  
 329 B6, B7, and B8 had crack patterns and failure modes as  
 330 shown in Fig. 6b. It can be noticed from the figure and  
 331 Table 9 that, generally, reducing  $a/d$  for Group B speci-  
 332 mens led to higher first crack flexural, shear loads, and  
 333 higher ultimate loads compared to those of Group A  
 334 specimens without changing the mode of failure. For  
 335 example, B5 had a first vertical crack at 31 kN which is  
 336 higher than that of B1 by 41%, and the failure was shear at  
 337 diagonal cracking load from the load application to the  
 338 support at 95.4 kN. With adding PVA 0.75%, B6, started  
 339 first vertical flexural crack at 47 kN which is higher than  
 340 that of B2 by 47%, and new flexural cracks were formed all  
 341 over the beam with the increment of loading. With further  
 342 increase in load, existing flexural cracks started to propa-  
 343 gate diagonally towards the loading point as well as new  
 344 diagonal cracks initiated separately away from the mid-  
 345 span along the beam at 148 kN. Increasing PVA% to 1.5%,  
 346 B7 behaved as B6 but with higher first crack vertical  
 347 flexural loads to 57 kN which is higher than that of B3 by  
 348 42.5%, and ultimate load to 232 kN. With a further  
 349 increase of PVA to 2.25%, B8 had a higher first vertical  
 350 flexural crack of 68 kN which is higher than that of B4 by



**Table 9** Comparison between experimental and NLFEA results

Group	Beam	Experimental results					NLFEA results					Experimental /NLFEA Results		
		$P_{cr, (flexural)}$ kN	$P_{cr, (shear)}$ kN	$P_u$ , kN	$\delta u$ , (mm)	$I^*$	$P_{cr, (flexural)}$ kN	$P_{cr, (shear)}$ kN	$P_u$ , kN	$\delta u$ , (mm)	$I^*$	$P_u$	$\delta u$ , (mm)	$I^*$
Group A	B1	22.0	27.0	89.5	3.0	161.0	18.0	20.0	82	3.1	145	1.091	0.955	1.110
	B2	32.0	38.0	134.3	3.7	285.0	25.0	30.0	138.75	3.76	279	0.968	0.987	1.022
	B3	40.0	50.0	170.0	3.92	363.0	31.0	38.0	176	4.3	384	0.966	0.917	0.945
	B4	48.0	60.0	203.3	4.4	504.0	36.0	49.0	203	5	540	1.002	0.880	0.933
Group B	B5	31.0	30.0	95.4	2.5	155.0	26.0	23.0	98	2.4	142	0.973	1.021	1.092
	B6	47.0	40.0	148.0	2.8	246.0	35.0	31.0	142	2.7	210	1.042	1.019	1.171
	B7	57.0	52.0	232.0	3.7	531.0	45.0	44.0	218	3.76	450	1.064	0.976	1.180
	B8	68.0	65.0	264.0	4.3	721.0	55.0	53.0	261	4.26	630	1.011	1.012	1.144
Group C	B9	46.0	60.0	189.0	4.1	500.0	35.0	45.0	181.5	3.98	416	1.041	1.030	1.202
	B10	50.0	60.0	201.0	4.2	552.0	35.0	52.0	183.5	3.88	450	1.094	1.075	1.227
	B11	50.0	70.0	234.5	4.22	617.0	40.0	56.0	219	3.92	510	1.071	1.07	1.210
Group D	B12	40.0	50.0	163.3	4.2	481.0	28.0	38.0	178	4.19	410	0.919	1.012	1.173
	B13	40.0	60.0	173.1	4.2	484.0	34.0	44.0	190.5	4.26	440	0.909	0.986	1.100
	B14	45.0	60.0	200.0	4.0	528.0	36.0	47.0	183	3.92	480	1.095	1.015	1.100
Group E	B15	33.0	48.0	118.0	3.2	250.0	27.0	38.0	128	2.9	215	0.921	1.103	1.160
	B16	35.0	55.0	138.0	3.6	320.0	29.0	42.0	155	3.3	280	0.890	1.090	1.143
	B17	39.0	55.0	170.0	3.7	510.0	32.0	46.0	181	3.55	450	0.939	1.042	1.133

$I^*$  energy absorption

351 42% and showed many small flexural cracks until the final  
352 diagonal shear cracking at ultimate load of 263.8 kN.

#### 353 4.2.3 Group C

354 Crack pattern, failure modes, and values of first cracks and  
355 ultimate loads of Group C specimens B9, B10, and B11  
356 with  $ald$  equals 2.25, PVA of 1.5%, and variable stirrups  
357 distribution are shown in Fig. 6c and recorded in Table 9. It  
358 can be seen from the figure and the table that the combina-  
359 tion of stirrups and PVA in test beams led to a more  
360 ductile behaviour compared to their companions in Group  
361 A with the same  $ald$ , the same PVA content and without  
362 stirrups. This can be observed from the increase of energy  
363 absorption values of Group C specimens compared with  
364 those of Group A ones. This was indicated by more vertical  
365 flexural cracks as shown in Fig. 6c and higher first crack  
366 flexural and shear loads. For example, B9 with 5 $\Phi$ 6/m  
367 stirrups had a first flexural crack load, first shear crack load  
368 and ultimate load of 46 kN, 60 kN, and 189 kN which are  
369 higher than those of B3 by 15%, 20%, and 11%, respec-  
370 tively. In addition, B10 with 7.5 $\Phi$ 6/m stirrups had a first  
371 flexural crack load, first shear crack load and ultimate load  
372 of 50 kN, 60 kN, and 200.8 kN which are higher than those  
373 of B3 by 25%, 20%, and 18%, respectively. Moreover, for  
374 B11 with 10 $\Phi$ 6/m stirrups and PVA of 1.5%, the first  
375 flexural crack load, first shear crack load and ultimate load

were 50 kN, 70 kN, and 234.5 kN which are higher than  
those of B3 by 25%, 40%, and 38%, respectively. All the  
beams in Group C failed in shear with a diagonal shear  
cracks similar to those in Group A but with a ductile  
behaviour in terms of several flexural cracks all over the  
beams as warnings prior to the large diagonal shear cracks  
at failure.

#### 4.2.4 Group D

Beam specimens of Group D, B12, B13, and B14 with  $ald$   
equals 2.25, PVA of 0.75%, and variable distribution of  
stirrups had crack patterns, failure modes, values of first  
cracks, and ultimate loads as shown in Fig. 6d and recor-  
ded in Table 9. It can be seen from the figure and the  
recorded values in the table that B12 with stirrups 5 $\Phi$ 6/m  
had first crack flexural load, first shear crack, and ultimate  
loads higher than those of its companion in Group A, B2  
without stirrups by 25%, 32%, and 22%, respectively. In  
addition Fig. 6d shows that B12 had the dominance of  
dense flexural cracks noticed until failure  $P_u$  compared with  
specimen B2 (Group A) in Fig. 6b which showed less  
flexural cracks. On the other hand, B13 with stirrups  
7.5 $\Phi$ 6/m had first flexural crack load, first crack shear load  
and ultimate load of 40, 60, and 173.1 kN which are almost  
similar to those of Group A, B3, without stirrups and 1.5%  
PVA. It is interesting to notice that B14 with 10 $\Phi$ 6/m



401 stirrups and 0.75% PVA shows almost same trend of crack  
 402 pattern and recorded values of first vertical flexural crack  
 403 load, first shear crack load and ultimate load almost the  
 404 same as B4 (Group A) without stirrups and 2.25% PVA.

#### 405 4.2.5 Group E

406 For Group E beam specimens B15, B16, and B17 of  $a/d$   
 407  $d = 2.25$  with stirrups only, the crack pattern, failure  
 408 modes, values of first cracks and ultimate loads are shown  
 409 in Fig. 6e and recorded in Table 9. It can be seen from the  
 410 figure and the table that the specimens without PVA  
 411 showed less ductility compared to the specimens in Groups  
 412 C and D which have the same  $a/d$  and contain both of PVA  
 413 and stirrups. This is observed in the values of energy  
 414 absorption of these specimens in Table 9. This was indi-  
 415 cated by less vertical flexural cracks as shown in Fig. 6e  
 416 and lower first crack flexural and shear loads. For example,  
 417 B15 with 5 $\Phi$ 6/m stirrups and no PVA had a first flexural  
 418 crack load, first shear crack load and ultimate load of 33  
 419 kN, 48 kN, and 118 kN which are lower than those of B12  
 420 with the same stirrups reinforcement and containing 0.75%  
 421 PVA by 18%, 4%, and 28%, respectively. In addition, B16  
 422 with 7.5 $\Phi$ 6/m stirrups had a first flexural crack load, first  
 423 shear crack load and ultimate load of 35 kN, 55 kN, and  
 424 138.0 kN which are lower than those of B13 which con-  
 425 tains 0.75% and the same stirrups reinforcement by 13%,  
 426 8%, and 20%, respectively. Moreover, for B17 with 10 $\Phi$ 6/  
 427 m stirrups, the first flexural crack load, first shear crack  
 428 load and ultimate load were 39 kN, 55 kN, and 170 kN  
 429 which are lower than those of B14 of the same stirrups  
 430 reinforcement and 0.75% PVA by 13%, 8%, and 15%,  
 431 respectively. Again, all the beams in Group E failed in  
 432 shear with a diagonal shear cracks similar to those in Group  
 433 A but the stirrups reinforcement added a ductile behaviour  
 434 especially for PVA of 0.75, and 1.5%. This was indicated  
 435 by several flexural cracks all over the beams as warnings  
 436 prior to the large diagonal shear cracks at failure.

437 It was observed that during load application, vertical  
 438 flexural cracks were first observed for all the groups except  
 439 Group B of  $a/d$  equals 1.5. These cracks were initiated at

440 the mid-span of all beams as expected. However, the  
 441 number and width of these cracks differ with variables such  
 442 as PVA inclusion and content, shear span to depth ratio,  
 443 and stirrups existence and distribution. All beams failed in  
 444 shear as they were designed according to ECP 203-2007  
 445 [24] to be very strong in flexure and very weak in shear to  
 446 assess the PVA fibre effect. Failure took place shortly after  
 447 dominant diagonal shear crack (within one shear span)  
 448 extended to the top fibre as shown in Fig. 6a–e. The angle  
 449 of inclination of the diagonal cracks ranged between 30°  
 450 and 40°. It is interesting to notice that the effect of PVA  
 451 fibres is comparable to the effect of the presence of shear  
 452 reinforcement or even better on the shear strength of the  
 453 studied beams. The results recorded in Table 9 and the  
 454 crack pattern in Fig. 6 show that the behaviour of B3 with  
 455 1.5% PVA and no shear reinforcement is comparable to  
 456 that of B17 with 10 $\Phi$ 6/m stirrups reinforcement and no  
 457 PVA fibres. Moreover, B4 with 2.25% PVA and no stirrups  
 458 showed higher first cracking loads and ultimate loads than  
 459 those of B17 with 10 $\Phi$ 6/m stirrups and no fibres.

460 The presence of PVA resulted in several cracks and  
 461 warnings before failure. The increase of PVA% resulted in  
 462 a higher tensile strength and, in turn, a significant  
 463 improvement in ductility. This agrees with the results of  
 464 Pan et al. [1] as presented in Table 10. It can also be  
 465 observed that the contribution of PVA towards increasing  
 466 shear capacity is similar to that of the stirrups. This agrees  
 467 with Qudah [27] who reported that PVA was effective in  
 468 replacing the stirrups reinforcement in mortar composites,  
 469 where the failure was ductile and was triggered by plastic  
 470 hinging in the beams. It is worth mentioning that for Group  
 471 B specimens of less  $a/d$ , beams had a first shear cracking  
 472 load that is slightly less than the first flexural vertical  
 473 cracking load, while the opposite was true for Group “A”  
 474 specimens. In addition, specimen B8 with the maximum  
 475 PVA, 2.25% showed the maximum ultimate load prior to  
 476 shear failure. Crack pattern of PVA-mortar beams were  
 477 similar to that observed by Hasib et al. [28] who studied the  
 478 shear resistance of composite beams made of two layers,  
 479 one layer of reinforced concrete and another layer of PVA-  
 480 mortar without shear reinforcement. They found that PVA-

**Table 10** Comparing the inclusion of PVA fibres on the behavior of Beams with Ordinary Mortar Beams in the present work and Pan et al. [1]

Pan et al. [1]			Present Work		
Fibre content (PVA) $V_f$ %	Enhancement in load-carrying capacity	Enhancement in the Tensile strength	Fibre content (PVA) $V_f$ %	Enhancement in load-carrying capacity %	Enhancement in ductility %
M14—0.0%	1.00	1.00	B1—0.0%	1.00	1.00
M15—1.20%	1.00	1.51	B2—0.75%	1.72	1.36
M8—1.30	1.40	1.58	B3—1.50%	2.18	1.69
M16—1.40	1.47	1.78	B4—2.25%	2.61	2.20
M20—1.60	1.57	2.33			

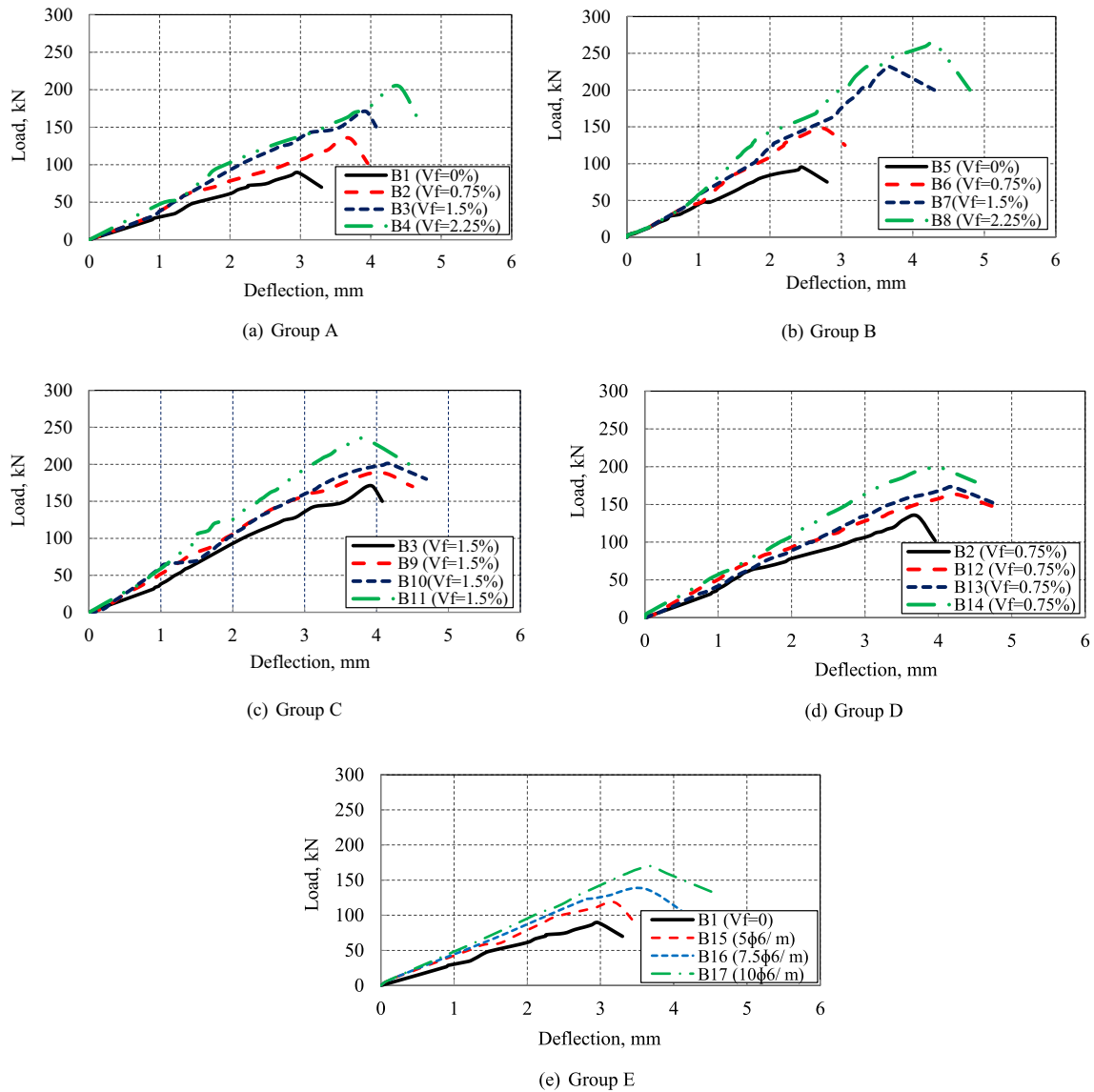


Fig. 7 Load–deflection curves for experimentally tested beams

481 mortar beams are superior in flexure and shear compared  
 482 normal reinforced concrete beams without PVA [26]. The  
 483 minimum increase in the ultimate load as a result of adding  
 484 PVA in the current study was 50% (B2) higher than that for  
 485 beams without PVA (B1), while the increase in the ultimate  
 486 load in PVA-mortar beams of Meng et al. [26] was  
 487 14.3% only over that of reinforced concrete beams without  
 488 PVA. This may be attributed to the effect of adding silica  
 489 fume to the binder in the current study.

### 490 4.3 Load–Deflection Relationships

491 Figure 7a–e shows the load–deflection relationships for the  
 492 test specimens comprising the five studied groups mentioned  
 493 in Table 7. It can be seen from the figures that,

generally, the load displacement for all the test specimens  
 494 exhibited similar pattern for the different studied groups  
 495 but with different ultimate loads and corresponding  
 496 deflections, based on the studied variables, namely *ald*,  
 497 PVA%, and presence of stirrups.  
 498

#### 499 4.3.1 Group A

For Group “A” specimens tested at *ald* equals 2.25, Fig. 7  
 500 a shows that adding PVA to the mix resulted in a significant  
 501 improvement in the performance of the studied beams  
 502 compared with the control one without PVA. This is  
 503 indicated by an increase in the ultimate load, and corre-  
 504 sponding deflection. In addition, increasing the percentage  
 505 of PVA resulted in a further improvement in the  
 506

507 performance. For example, specimen B1 with no PVA had  
508 an ultimate load and corresponding deflection of 89.5 kN,  
509 and 3 mm, respectively. For specimens B2 with PVA%  
510 equals 0.75%, B3 with PVA% equals 1.5% and B4 with  
511 PVA% equals 2.25%, the ultimate loads were higher than  
512 that of specimen B1 by 50%, 92% and 157%, and their  
513 corresponding deflections were higher than that of speci-  
514 men B1 by 24%, 31%, and 47.3%, respectively.

#### 515 4.3.2 Group B

516 The load–deflection curves for Group “B” specimens tes-  
517 ted at  $a/d$  equals 1.5 are shown in Fig. 7b. It can be seen  
518 from the figure that generally, the specimens of  $a/d$  equals  
519 1.5 showed higher ultimate loads compared with those of  
520 specimens of higher  $a/d$  (2.25) shown in Fig. 7a. For  
521 example, Fig. 7b shows that Specimen B5 without PVA  
522 had an ultimate load of 95.35 kN which is higher than that  
523 of B1 (Group A) of  $a/d$  equals 2.25 by 7%. Figure 7b  
524 shows also that specimens B6 with PVA% equals 0.75%,  
525 B7 with PVA% equals 1.5% and B8 with PVA% equals  
526 2.25%, had ultimate loads higher than that of specimen B5  
527 by 55%, 144% and 177%, and their corresponding  
528 deflections were higher than that of specimen B5 by 16.3%,  
529 44%, and 75.9%, respectively.

#### 530 4.3.3 Group C

531 The load deflection curves of Group “C” specimens of  
532 specific content of PVA, 1.5%, presence of stirrups, and  $a/$   
533  $d$  equals 2.25 are shown in Fig. 7c. It can be seen from the  
534 figure that the combined effect of stirrups and PVA  
535 resulted in a slight improvement in the performance of  
536 studied beams compared with that of beam B3 which  
537 included PVA without stirrups. Figure 7 (c) shows that  
538 specimens B9 with stirrups 5 $\phi$ 6/m, B10 with stirrups 7.5 $\phi$   
539 6/m, and B11 with stirrups 10 $\phi$ 6/m had ultimate loads  
540 higher than that of specimen B3 (Group A) of the same  
541 PVA percentage and without stirrups by 17%, 18% and  
542 38% and their corresponding deflections were higher than  
543 that of specimen B3 by 5.20%, 7.30%, and 8.50%,  
544 respectively.

#### 545 4.3.4 Group D

546 Figure 7d shows the load deflection curves for Group “D”  
547 specimens with less percentage of PVA, 0.75%, and pres-  
548 ence of stirrups. It can be seen from Fig. 7d that generally  
549 the ultimate loads are less than those of the specimens with  
550 the same stirrups areas and higher PVA, 1.5% in Fig. 7c. It  
551 can be seen from Fig. 7d that the ultimate loads and cor-  
552 responding deflections of the beams including PVA and  
553 stirrups are higher than those of B2 with the same PVA

percentage and without stirrups. In addition, these values  
554 increased with increasing the area of the stirrups. For  
555 example, the ultimate loads of specimens B12, B13 and  
556 B14 were higher than those of B2 (Group A) without  
557 stirrups by 13%, 15% and 31.5%, while their correspond-  
558 ing deflections were higher than those of specimen B2 by  
559 13%, 13%, and 7%, respectively. 560

#### 561 4.3.5 Group E

562 The load–deflection curves for Group “E” specimens with  
563 no PVA, and with different stirrups reinforcement distri-  
564 bution are shown in Fig. 7e. It can be seen from the fig-  
565 ure that generally the ultimate loads of Group “E”  
566 specimens are higher than that of the control beam B1 of  
567 Group “A” without fibres and stirrups. In addition, Table 9  
568 shows that the first cracking flexural and shear loads of  
569 B15–B17 of Group “E” are almost similar to those of B2  
570 and B3 of Group “A” which contain 0.75% and 1.5% PVA  
571 and no stirrups. Moreover, the first flexural and shear  
572 cracking loads of B4 which contains 2.25% PVA and no  
573 stirrups was higher than that of B17 of Group “E” with  
574 10 $\phi$ 6/m stirrups and no fibres. The ultimate loads of  
575 specimens with no shear reinforcement (Group A), B2  
576 (0.75 & PVA), B3 (1.5% PVA) and B4 (2.25% PVA) were  
577 higher than those of specimens with no PVA (Group E),  
578 B15 (5 $\phi$ 6/m), B16 (7.5 $\phi$ 6/m), and B17 (10 $\phi$ 6/m) by 12%,  
579 19% and 16%, respectively.

580 It can be seen from the above results and the curves  
581 shown in Fig. 7a–e that the inclusion of PVA fibres led to  
582 an increase in the tensile strength of test beams which, in  
583 turn, improved shear resistance by raising the cracking  
584 loads and ultimate loads compared to beams without PVA  
585 as indicated in Table 9. In addition, the combination of  
586 PVA fibres and the stirrups (transverse) reinforcement  
587 contributed to the shear behaviour of studied beams.  
588 Moreover, specimens containing PVA fibres and without  
589 shear reinforcement have higher ultimate loads than those  
590 with shear reinforcement and without PVA fibres. Com-  
591 parison of the results showed that the effect of PVA fibres  
592 on the ultimate loads (shear capacity) and corresponding  
593 deflections was more significant for lower shear span-to-  
594 depth ratio ( $a/d$ ) and with reducing the amount of shear  
595 reinforcement. Shimizu et al. [29] also showed that the  
596 shear strength of steel reinforced PVA-mortar beams  
597 increased with the increase in volume percentage of PVA  
598 fibre. For beams of  $a/d$  equals 1.5 and containing PVA  
599 equals 2%, Shimizu et al. [29] found that the increase of  
600 ultimate load was 80% higher than their companion of  
601 normal concrete without PVA, while the beams of the  
602 current study of the same  $a/d$  and containing PVA equals  
603 2.25%, the increase in ultimate load was 177% compared  
604 to beams without PVA. This may be attributed to the

605 combined action of PVA fibres and cement replacement  
606 materials, fly ash and silica fume, which formed the mortar  
607 composites in the current study.

#### 608 4.4 Energy Absorption (*I*)

609 Energy absorption was defined as the area under load–  
610 deflection curves and it is a good indication to measure the  
611 ductility of structural elements [30]. It can be seen from  
612 Fig. 7a–e and Table 9 that, generally, the energy absorption  
613 was enhanced by increasing PVA fibre content. In addition,  
614 the combination of stirrups and PVA improved the ductility  
615 of studied specimens. Moreover, the shear span to depth  
616 ratio has a significant effect on the ductility of specimens.  
617 The maximum energy absorption was observed for Group  
618 B of *ald* equals 1.5 especially for Specimen B8 where the  
619 PVA% equals 2.25% and without stirrups. For example,  
620 Fig. 7a and Table 9 show that for Group A with *ald* equals  
621 2.25 and no stirrups, the energy absorption for specimens  
622 B2, B3 and B4 were higher than that of B1 by 77%, 125%  
623 and 213%, respectively. With reducing the *ald* to 1.5,  
624 Fig. 7b and Table 9 show that Group B specimens, B6, B7,  
625 and B8 had energy absorptions of 59%, 243% and 365%  
626 higher than that of specimen B5 without PVA. For Group C  
627 with 1.5% PVA and presence of stirrups, Fig. 7c and  
628 Table 9 show that the enhancement of energy absorption of  
629 specimens B9, B10, and B11 was higher than that of  
630 specimen B3 of the same content of PVA and without  
631 stirrups by 38%, 52%, and 70%, respectively. For Group D  
632 specimens with less PVA, 0.75%, and presence of stirrups,  
633 Fig. 7d and Table 9 show that the energy absorptions of  
634 specimens B12, B13, and B14 were higher than that of B2  
635 by 69%, 70%, and 85%, respectively. For Group E speci-  
636 mens with no PVA and stirrups only, Fig. 7e and Table 9  
637 show that the energy absorptions of B15 and B16 with  
638 stirrups only were lower than those of B2 and B3 with PVA  
639 fibres only by 12.1% and 11.8%, respectively.

640 Enhancement of energy absorption was observed for  
641 PVA-mortar beams. This implies that the number of stir-  
642 rups could be reduced when the PVA is added to the mortar  
643 matrix in a reasonable percentage (minimum 1.5%). The  
644 shear behaviour of beams without stirrups (shear rein-  
645 forcement) was studied by Ismail and Hassan [13]. They  
646 reported that the PVA-mortar beams showed better per-  
647 formance in terms of cracking behaviour, shear capacity,  
648 ductility and energy absorption compared with the con-  
649 ventional reinforcement concrete beam. In addition, Hos-  
650 sain et al. [31] reported that PVA-mortar was effective in  
651 replacing the stirrups reinforcement and the energy  
652 absorption was improved for specimens containing PVA  
653 compared with self-consolidating concrete (SCC) beam  
654 specimens of *ald* equals 1.53. They found that the energy  
655 absorption for PVA-mortar beams was higher than that for

SCC by 100% for beams without stirrups reinforcement,  
while, in the current study, the energy absorption for PVA-  
mortar beams of the same *ald*, B7 with 1.5% PVA was  
higher than that of B5 with no PVA by 242%. The drastic  
improvement of the results of PVA-mortar beams in the  
current study revealed the significance of combining fly  
ash, silica fume with PVA fibres.

#### 663 4.5 Load–Strains Relationships

664 The strains in the longitudinal tension bars and stirrups  
665 reinforcement were measured as explained in Sects. 3.3  
666 and 3.4. The load strain relationships for longitudinal bars  
667 in studied specimens are shown in Fig. 8a–e and the load  
668 strain curves for stirrups are shown in Fig. 9a–c.

##### 669 4.5.1 Load–Strain Curves for Longitudinal Reinforcement

670 As was observed previously for the crack pattern and  
671 failure modes in Sect. 4.1, all PVA-mortar beams have  
672 failed in shear. This was indicated in Fig. 8a–e that the  
673 maximum loads recorded for longitudinal tension bars  
674 were less than the ultimate shear load at failure, recorded in  
675 Table 9, and the corresponding strains were all less than the  
676 yield value. For example, it can be seen from Fig. 8a that  
677 for Group A specimens, B1, B2, B3, and B4, the maximum  
678 load was 195 kN for B4 which is lower than the ultimate  
679 shear load recorded in Table 9 (204 kN), while the maxi-  
680 mum strain was 0.0009 for B2. Figure 8b shows that the  
681 maximum load for B8 of *ald* equals 1.5 was 240 kN which  
682 is lower than ultimate shear load recorded in Table 9 (264  
683 kN) and corresponding strain was 0.00125 which is higher  
684 than that for its companion B4 of *ald* equals 2.25 by 78.6%.  
685 On the other hand, Fig. 8c–e show that the maximum load  
686 at longitudinal reinforcement are almost the ultimate loads  
687 recorded in Table 9 and the corresponding strains of  
688 Groups C, D, and E specimens with stirrups are more than  
689 double as much those of Groups A and B specimens which  
690 indicate the shear failure shown previously in crack pattern  
691 and failure modes. For example, Fig. 8c, Group C speci-  
692 mens of PVA (1.5%) had maximum load equals 234 kN  
693 and the corresponding strain was 0.0023 for B11 which are  
694 higher than those of its companion B3 of the same PVA  
695 content without stirrups by 42% and 233%, respectively. In  
696 addition, Fig. 8d shows that the maximum load was 200 kN  
697 for B14, while maximum strain was 0.0022 for B12 which  
698 is higher than that of its companion B2 without stirrups in  
699 Group A by 144.4%. Moreover, Fig. 8e shows that the  
700 maximum load was 170 kN for B17, while maximum strain  
701 was 0.002 for B15 which is higher than the maximum  
702 strains of the beams in Group A. This may be attributed to  
703 the fact that the presence of stirrups in Groups C, D (in  
704 combination with PVA-mortar) and in Group E contributed

705 to resist shear stresses which led to further action of longi-  
 706 tudinal reinforcement in flexure which resulted in higher  
 707 strains in longitudinal bars.

#### 708 4.5.2 Load–Strain Curves for Stirrup Reinforcement

709 Figure 9a–c shows the load–strain relationships for stirrups  
 710 reinforcement in Groups C, D, and E. It can be seen from  
 711 the figures that, for all specimens with stirrups, the strains  
 712 along the stirrups exceeded the yield value. In addition, the  
 713 maximum loads at stirrups and corresponding strains for  
 714 specimens in Group C containing PVA equals 1.5% are  
 715 higher than those of Group D with PVA equals 0.75% and  
 716 those of Group E without PVA fibres. For example, B9 in  
 717 Group C had a maximum load of 155 kN and corre-  
 718 sponding stirrups strain of 0.0062 which are higher than

719 those of B12 in Group D by 0% and 26.5% and those of  
 720 B15 in Group E by 24% and 19%, respectively. In addition,  
 721 B10 in Group C had a maximum load at stirrups of 200 kN  
 722 and corresponding stirrup strain of 0.0064 which are higher  
 723 than those of B13 in Group D by 14.3% and 60%, and  
 724 those of B16 in Group E by 30.5% and 30%, respectively.  
 725 Moreover, B11 in Group C had a maximum load of 240 kN  
 726 and corresponding stirrup strain of 0.0059 which are higher  
 727 than those of B14 in Group D by 20% and 9.2%, and higher  
 728 than those of B17 in Group E by 29.1% and 17%,  
 729 respectively. It can be argued that the improvement of  
 730 ductility of studied beams as a result of the combination of  
 731 PVA of 1.5% with stirrups was higher than that for the  
 732 combination of half content of PVA (0.75%) with the same  
 733 amount of stirrups or their companions with stirrups only.  
 734 In other words, increasing PVA% resulted in improvement

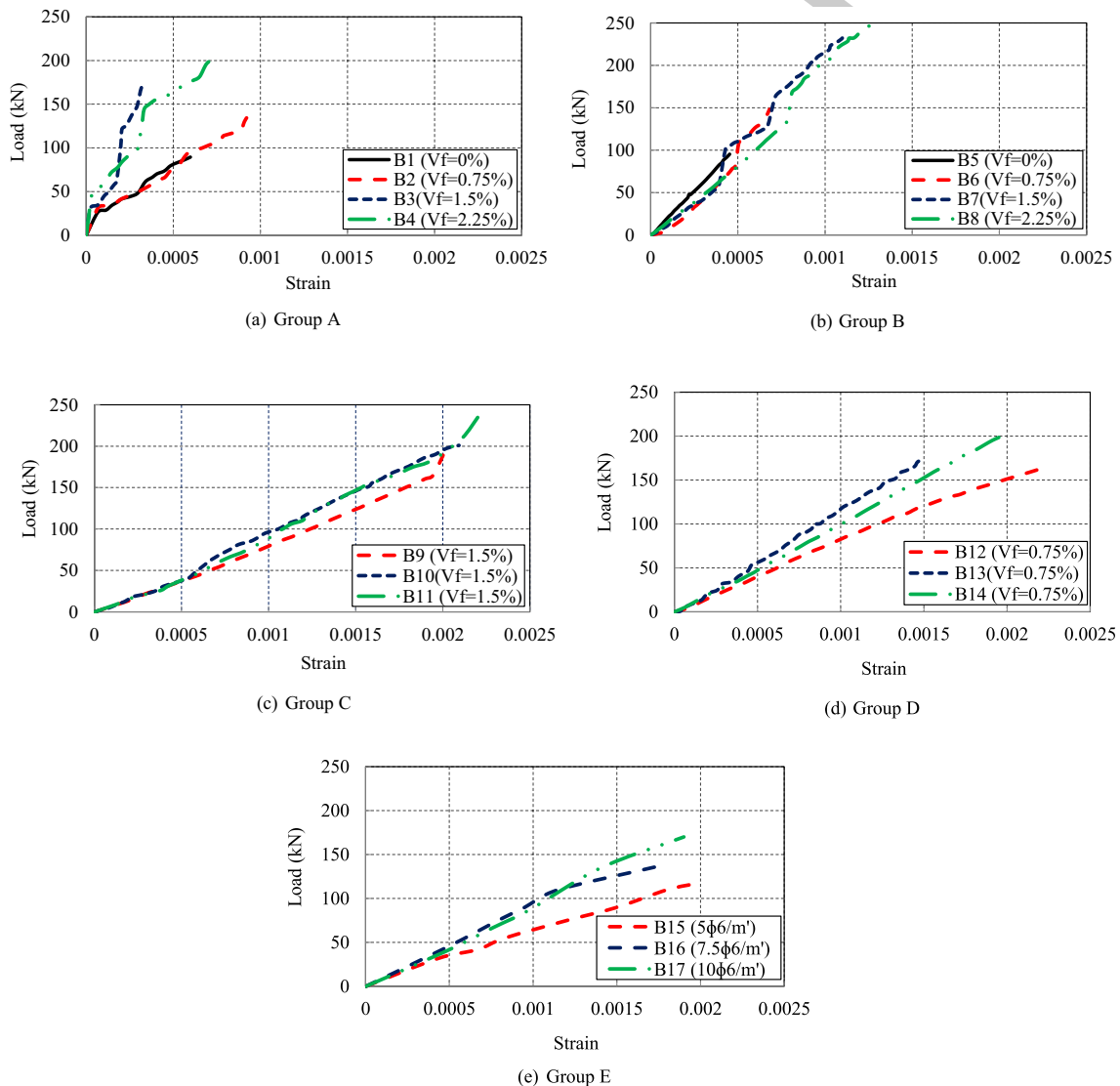


Fig. 8 Load–strain curves for longitudinal reinforcement

735 of shear strain and this improvement is more significant for  
736 beams without stirrups. In their study of the shear behav-  
737 iour of steel reinforced PVA-mortar beams, Hasib and  
738 Hossain [28] reported that the average shear strain in shear  
739 crack surface at maximum strength is highly influenced by  
740 differences of volume percentage of PVA fibre.

741 From the above results, the authors recommend a  
742 combination of at least 1.5% PVA and stirrups reinforce-  
743 ment (minimum  $5\Phi 6/m$ ) to achieve adequate shear behav-  
744 iour of PVA-mortar beams. This combination prevented  
745 sudden failure and improved the ductility as several small  
746 flexural cracks were formed prior to failure. The effect of  
747 both of PVA% and transverse reinforcement ratio % on the  
748 ultimate loads of the studied beams is shown in Fig. 10. It  
749 can be seen that at the same percentage, the PVA has  
750 higher effect on the ultimate load compared to that of  
751 transverse reinforcement.

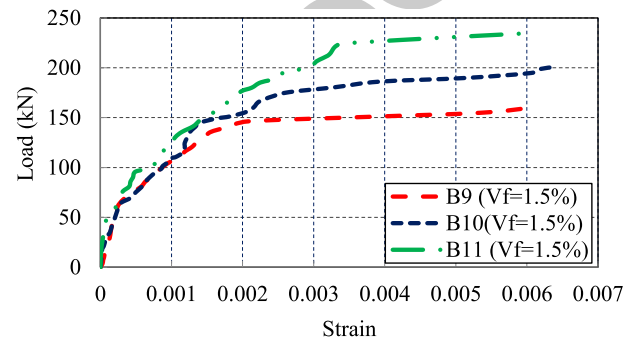
## 752 5 Non-linear Finite Elements Analysis 753 (NLFEA)

754 The experimentally tested PVA-reinforced mortar beams  
755 were modelled using the non-linear finite element package  
756 ANSYS 14.5 [32] to predict the structural behaviour. The  
757 load–deflection relationships and the crack patterns for test  
758 beams were conducted to verify the numerical modelling  
759 with the obtained experimental results. Based on the  
760 ANSYS program manual, the finite element modelling of  
761 mortar, PVA fibres, and steel in PVA-reinforced mortar  
762 beams are briefly described in the following sections.

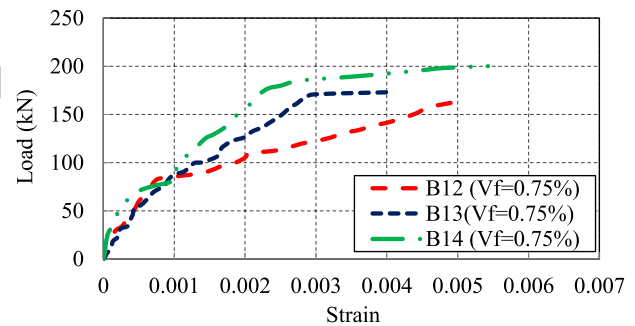
### 763 5.1 Modeling of Test Beams

764 In the finite element discretization of each beam, a mesh of  
765 average size  $25 \times 25 \times 20$  mm of eight-node elements  
766 was used for all beams. The area and spacing of bar ele-  
767 ments were similar to those used in the experimental  
768 specimens. The concentrated loads were also applied to the  
769 top surface at mid-span of the tested beams. The supports  
770 were represented by restrained nodes at the corresponding  
771 locations. The structural element type used for geometric  
772 idealization of the mortar is Solid 65 as its capability to the  
773 plastic deformation, cracking and crushing in three direc-  
774 tions. The PVA fibres were simulated as smeared rein-  
775 forcements in Solid 65 element represented through  
776 volumetric ratio to represent the actual fibre volumes used  
777 in each beam specimen [33]. It is defined by eight nodal  
778 points as shown in Fig. 11. Stress–strain curves in mortar  
779 in compression which are shown in Fig. 5 and the prop-  
780 erties of PVA-mortar composites recorded in Table 8 were  
781 used in the model.

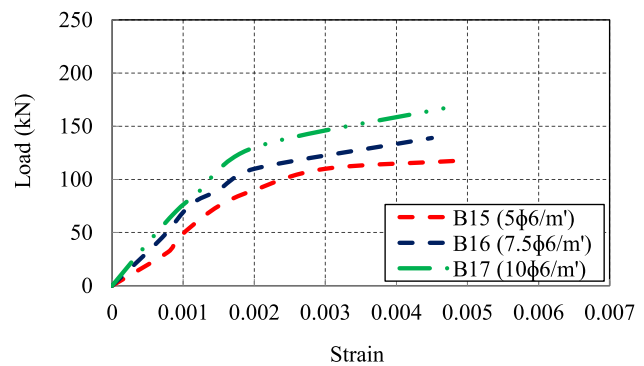
782 Longitudinal steel reinforcement and stirrups were  
783 modeled using the ANSYS 3D Spar LINK 180 elements as  
784 shown in Fig. 12. The element is a uniaxial tension–com-  
785 pression element with three degrees of freedom at each  
786 node. The material properties of the steel reinforcement  
787 have been obtained from the experimental testing. The  
788 steel yield strength, elastic modulus and Poisson’s ratio  
789 were taken as 450 MPa, 200 GPa and 0.3, respectively. The  
790 average stress–strain curve developed earlier [34] for steel  
791 bars embedded in concrete is used in the current research  
792 (see Fig. 13). The stress–strain relationship is expressed by  
793 two straight lines and the non-linear behaviour of steel was



(a) Group C



(b) Group D



(c) Group E

Fig. 9 Load–strain curves for stirrups

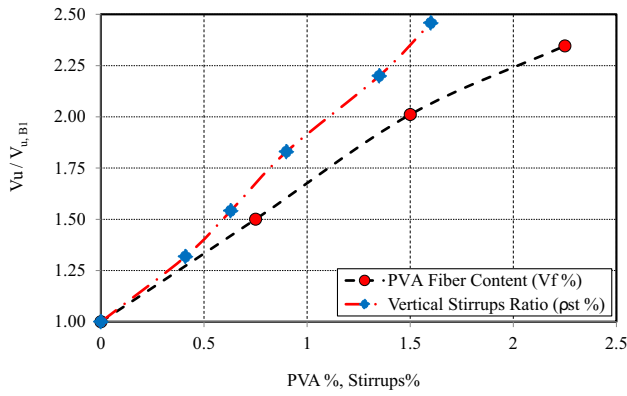


**Fig. 10** Effect of PVA-Fiber content ( $V_f$  %) and transverse reinforcement ratio ( $\rho_{st}$  %) on the ultimate capacity of studied beams

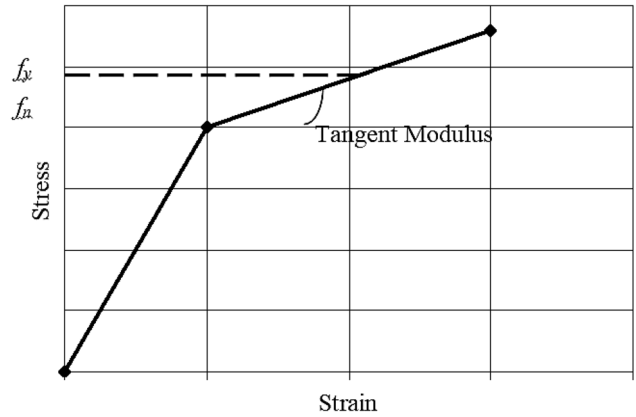


**Fig. 13** Stress-strain curve for steel reinforcement [32]

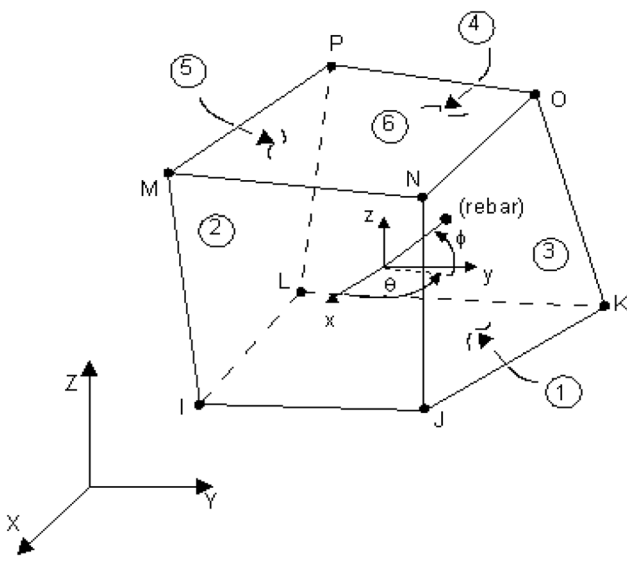


**Fig. 11** Geometry of 3-D Solid 65 Element [30]

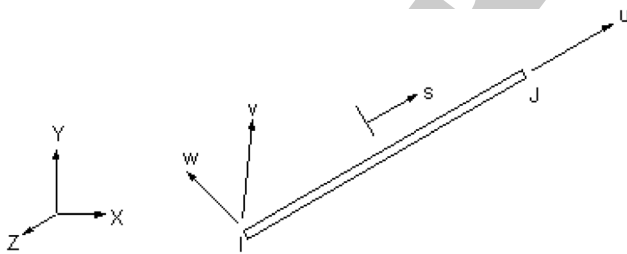


**Fig. 12** 3-D Spar LINK 180 element [30]

794 modeled as bilinear. Solid 45 was idealized at the location  
 795 of loading and supports in the concrete beams to avoid  
 796 stress concentration problems. Figure 14 shows the typical  
 797 idealization of the Composite PVA-mortar composites and  
 798 steel elements for the tested beams used in the analysis.

## 5.2 Prediction of Crack Pattern and Load-Deflection Results

Figure 15 shows the comparison between experimental and predicted crack pattern at failure for typical specimens, namely, B4 and B12. It can be seen from the figure that the developed cracks in the PVA-mortar beam specimens are well distributed through the whole span. The shear stresses increases with increasing the load increment, start to induce diagonal cracks, and the shear failure was recorded. Good agreement was observed between the simulated crack patterns and the obtained experimental ones. The simulation also successfully predicted the sequence in the crack pattern development and the failure mechanism.

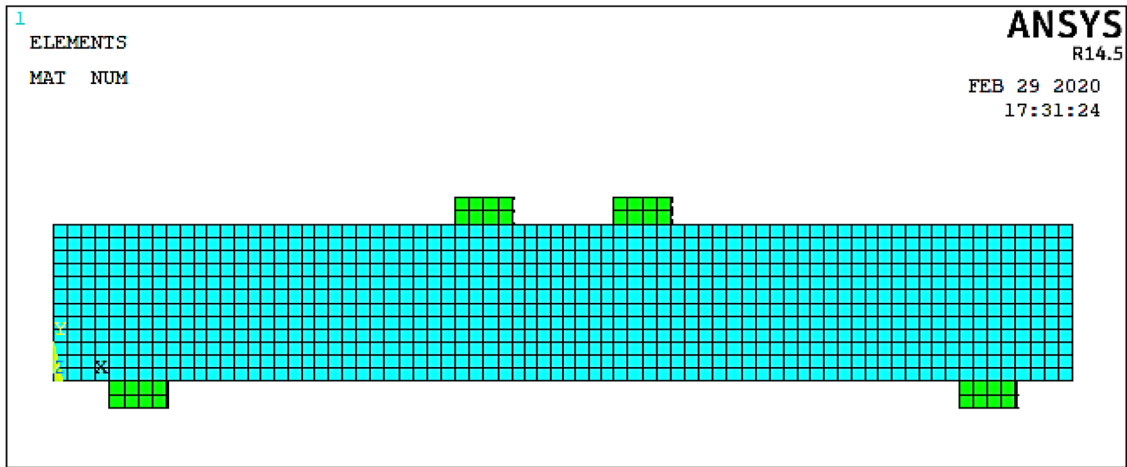
Figure 16 shows the numerical load deflection curves for the studied beams compared with the experimental ones for all beam specimens. It can be seen from the figure that, generally, the load-deflection relationships for all specimens exhibited similar features and the predicted load-deflection curves of most of the specimens were very close to the experimental ones. As ANSYS can measure the load-displacement until the failure only [32], its prediction does not show a reduction in the load after reaching the ultimate value compared with the experimentally obtained value. Values of experimental and numerical first crack flexural loads ( $P_{cr, M}$ ), first crack shear loads ( $P_{cr, S}$ ), ultimate loads ( $P_u$ ), ultimate displacements ( $\delta_u$ ), and energy absorption ( $I$ ). In addition, a comparison between predicted and experimental ultimate loads, corresponding displacements and energy absorption of the test specimens is given in Table 9. A very good agreement between the experimental results and the numerical ones was observed. The ratio of the predicted to experimental ultimate loads, corresponding displacements, and energy absorptions ranged between 0.89–1.095, 0.88–1.10, and 0.93–1.22, respectively.

799  
800

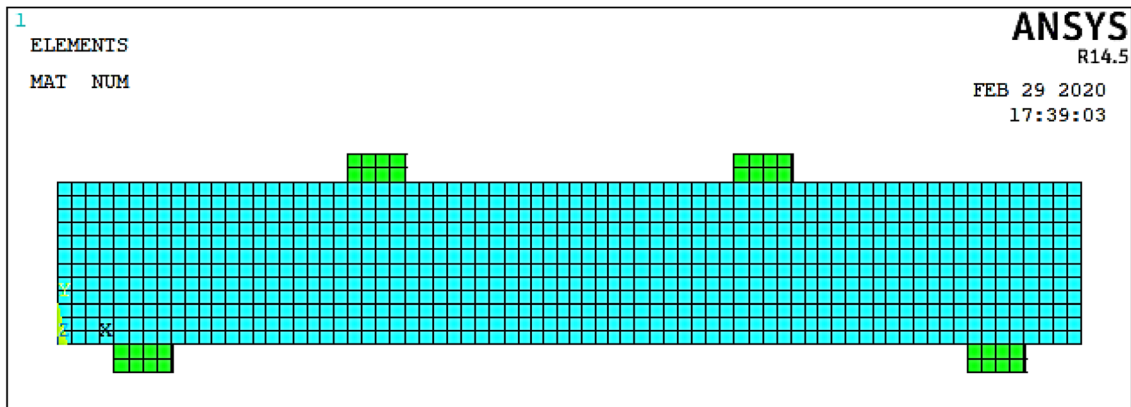
801  
802  
803  
804  
805  
806  
807  
808  
809  
810  
811

812  
813  
814  
815  
816  
817  
818  
819  
820  
821  
822  
823  
824  
825  
826  
827  
828  
829  
830  
831  
832  
833

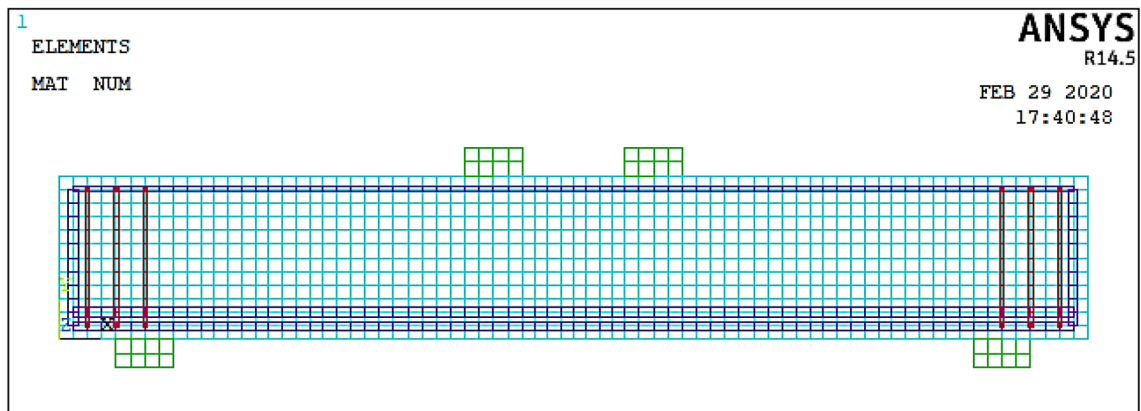




Specimens with  $a/d= 2.25$

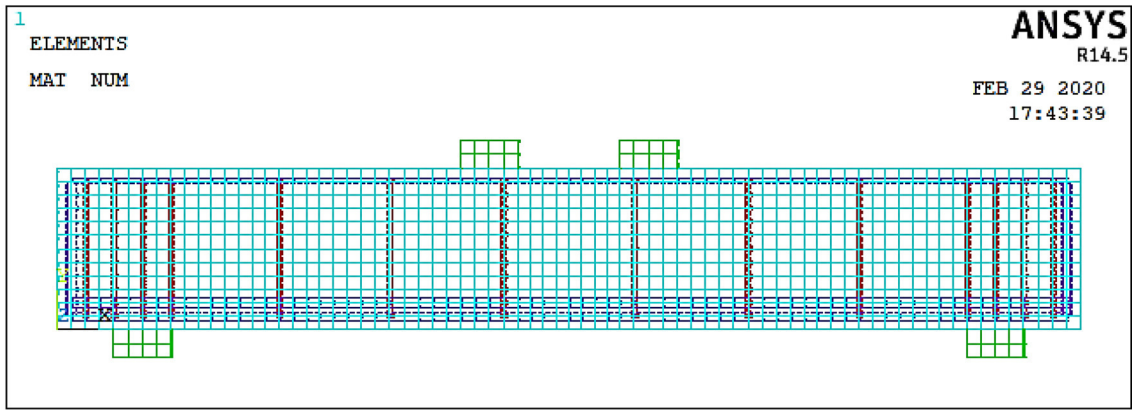


Specimens with  $a/d= 1.50$

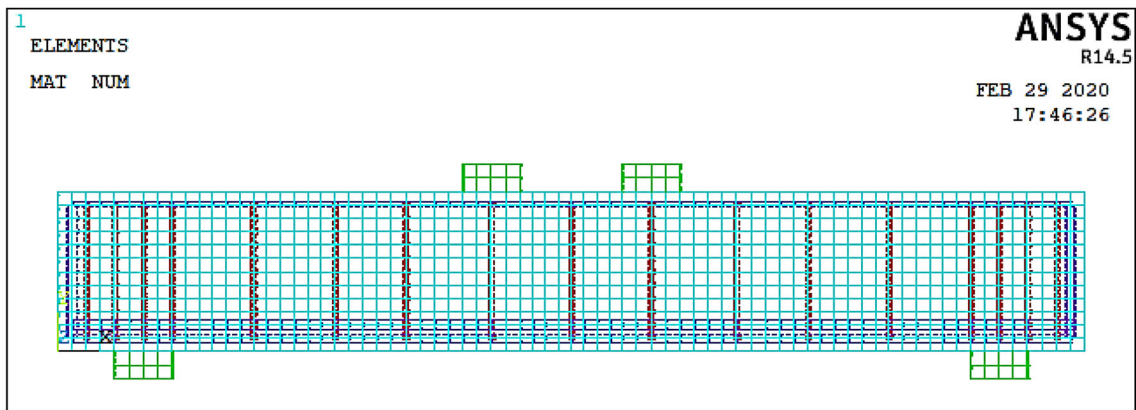


Specimens without Stirrups

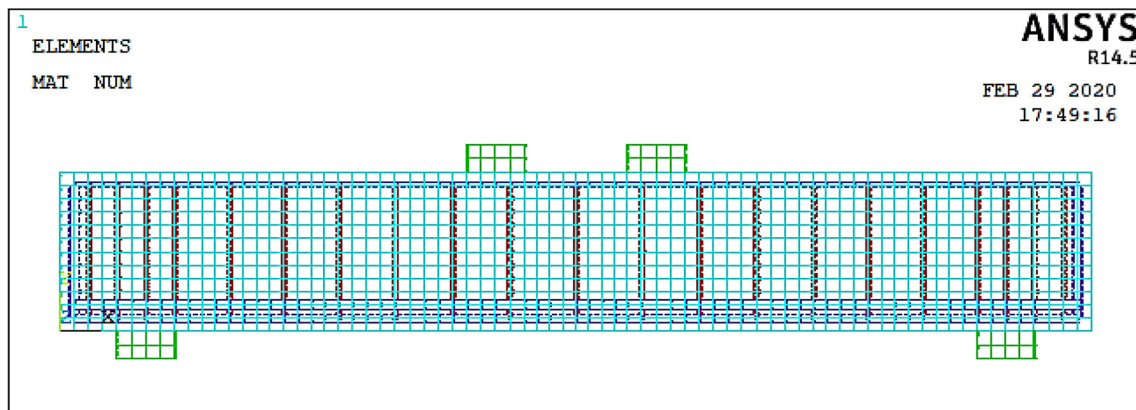
Fig. 14 Finite element modeling of test beams



Specimens with Stirrups  $5\phi 6/m'$

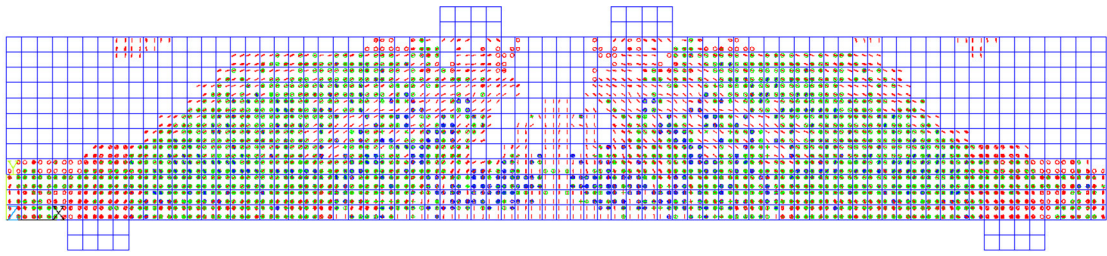


Specimens with Stirrups  $7.5\phi 6/m'$

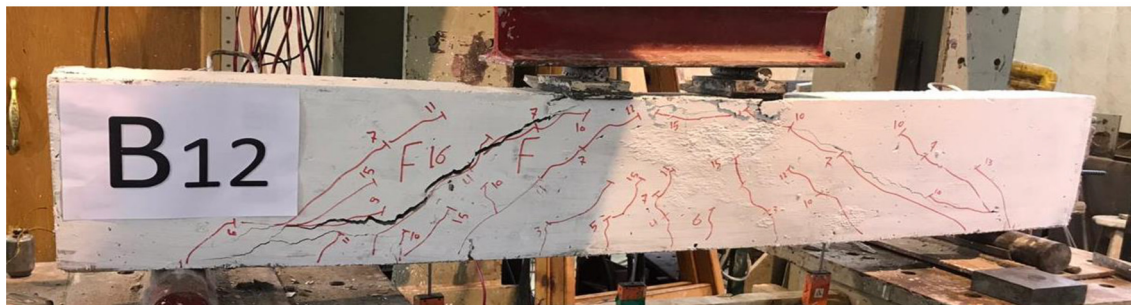
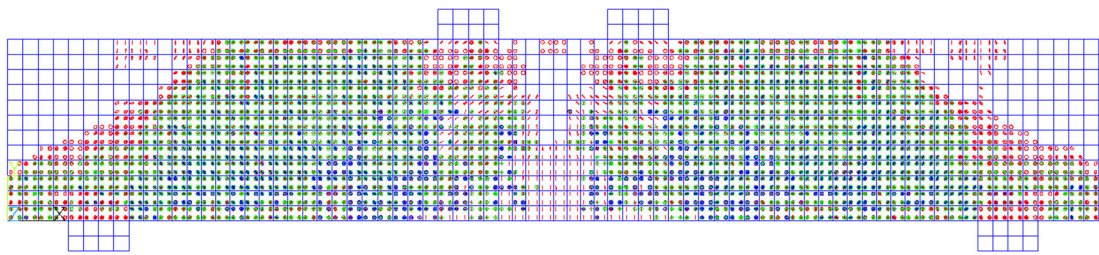


Specimens with Stirrups  $10\phi 6/m'$

Fig. 14 continued



(a) B4



(b) B12

Fig. 15 Predicted crack pattern for selected beams at failure

834 It can be seen that within the range of the test parameters  
 835 investigated, the application of the non-linear finite ele-  
 836 ment model, developed in this study, yielded satisfactory  
 837 first shear and flexural cracking loads, ultimate capacity  
 838 and deflections, load–deflection relationships, and energy  
 839 absorptions.

## 6 Prediction of Ultimate Shear Strength

The predicted analytical ultimate shear strength ( $V_{u, Anal.}$ ) for PVA-Mortar beams was performed to be compared with the experimental test results. A proposed equation was developed in the current research which is an enhancement

840

841

842

843

844

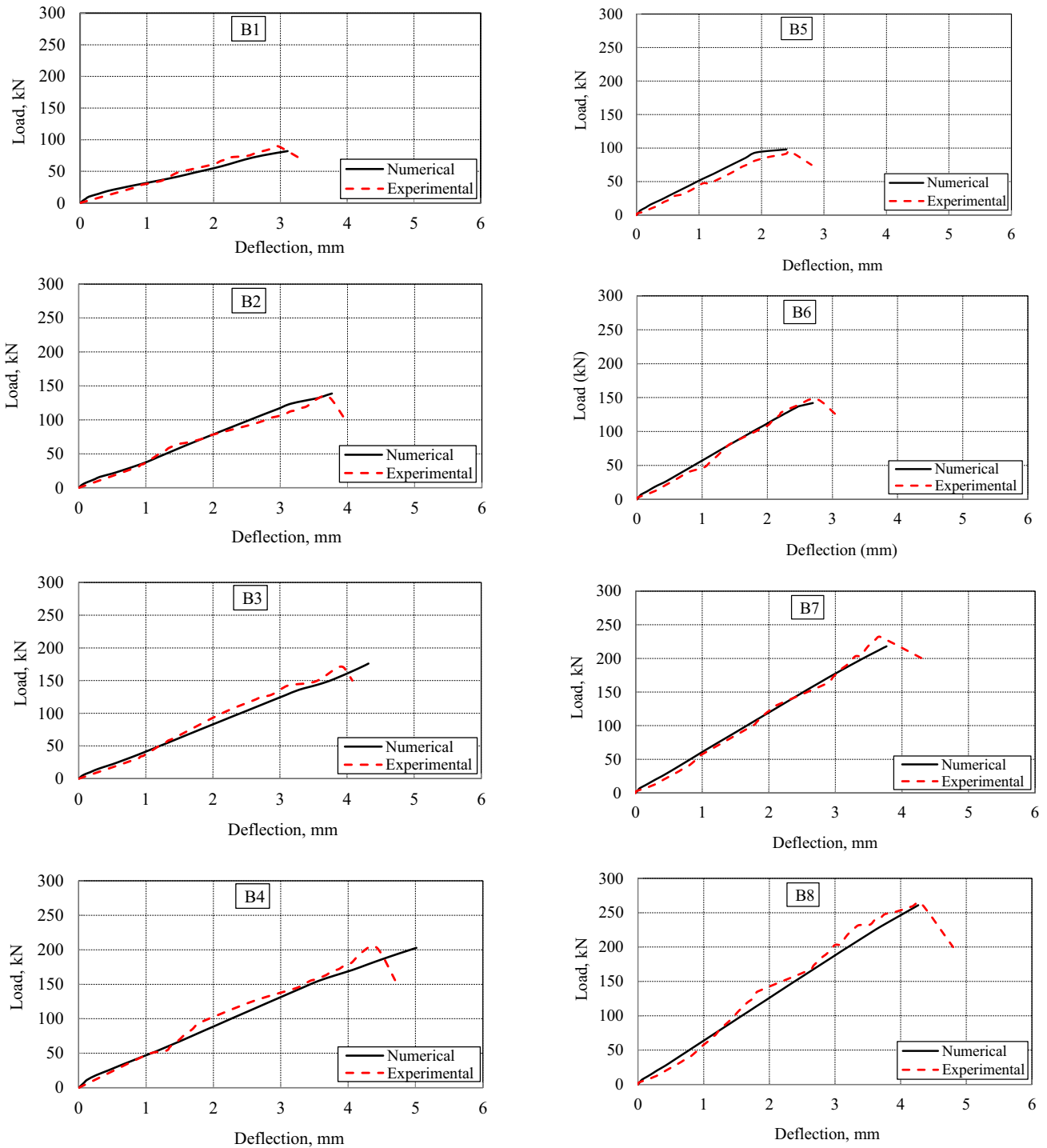


Fig. 16 Finite element prediction of load–deflection curves for test beams

845 equation of CSA Standard [35]. The ultimate shear strength  
 846 was predicted for a typical rectangular beam of a cross-  
 847 section ( $b \times t$ ) as follows:

$$V_{u,Anal.} = V_c + V_f + V_s. \quad (1)$$

The contribution of concrete to the shear resistance ( $V_c$ )  
 can be estimated by the empirical equation of CSA Stan-  
 dard [35] as follows:

$$V_c = (\Phi_c \lambda \beta \sqrt{f'_c}) b d_v, \quad (2)$$

849  
 850  
 851

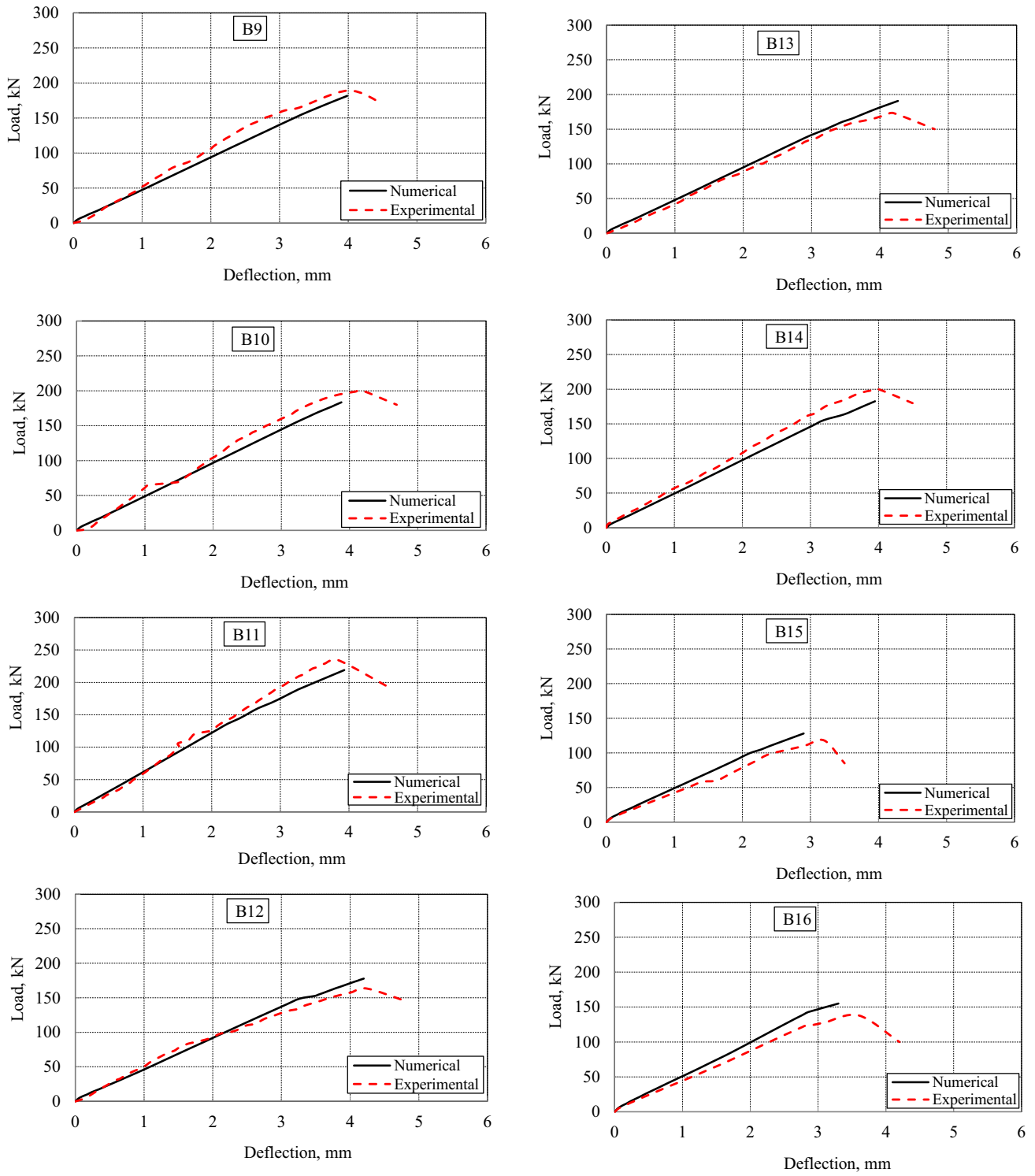


Fig. 16 continued

853 where the value of the factors  $\phi_c$ ,  $\lambda$ , and  $\beta$  are 0.65, 1.0, and  
 854 0.21, respectively. In addition, the value of  $d_v$  was taken as  
 855 the maximum of 0.9 the effective depth ( $d$ ) or 0.75 the  
 856 section depth ( $t$ ) [35].

The contribution of PVA fibres to shear resistance ( $V_f$ ) 857  
 can be predicted as follows: 858

$$V_f = F_{PVA} \beta_o \tau_b d_v. \quad (3)$$

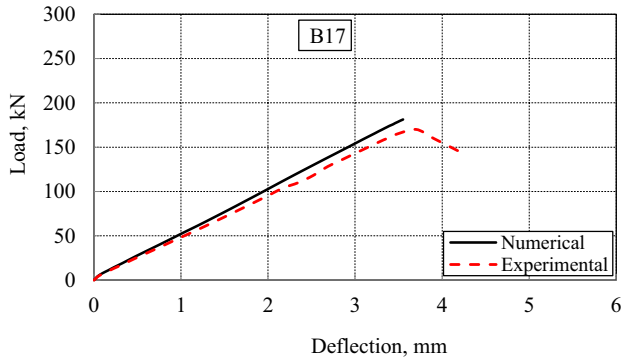


Fig. 16 continued

860 The fiber factor for PVA fibres ( $F_{PVA}$ ) is considered as  
861 [36]:

$$F_{PVA} = V_{F,PVA} \frac{l_f}{\phi_f} \lambda_f, \quad (4)$$

863 where ( $V_{F,PVA}$ ) is the percentage volume of PVA fibres,  
864  $l_f$  is the fiber length (12 mm),  $\phi_f$  is the fiber diameter  
865 (0.04 mm), ( $l_f/\phi_f$ ) is the PVA fibres aspect ratio, and  $\lambda_f$  is  
866 the shape factor with value of 0.5 [36]. In addition, the  
867 orientation factor ( $\beta_o$ ) is considered 0.41 [36], and the  
868 interface frictional bond of PVA fibres ( $\tau$ ) is taken as  
869 2.93 MPa [37].

870 The contribution of vertical stirrups in shear ( $V_s$ ) can be  
871 defined as follows [35]:

$$V_s = \Phi_s \frac{A_v}{S} f_{ys} b d_v, \quad (5)$$

873 where  $A_v$  is the area of the vertical stirrups,  $f_{ys}$  is the  
874 yield stress of the stirrups, the value of the factors  $\phi_s$  is  
875 taken as 0.85, and spacing between the stirrups ( $S$ ) was  
876 variable for the different specimens used in this investi-  
877 gation (B9–B17). Accordingly, the ultimate shear strength  
878 ( $V_{u, Anal.}$ ) can be predicted from Eq. (1). The analysis  
879 procedure for calculating  $V_{u, Anal.}$  can be easily imple-  
880 mented by hand calculations or a spreadsheet. Table 11  
881 presents a comparison between the experimental and pre-  
882 dicted ultimate shear strength. Good agreement was  
883 achieved between the experimental and predicted shear  
884 strength results. The overall average value of the ratio  
885 [ $V_{u, exp.}/V_{u, Anal.}$ ] for the studied beams is 1.038 with a  
886 standard deviation of 0.11 and the coefficient of variation  
887 equals 10.50%.

## 888 7 Conclusions

889 The current study aimed to investigate the shear behaviour  
890 of PVA-mortar beams. The studied variables were different  
891 percentages of PVA fibres (0.75%, 1.5%, and 2.25%),

shear span to depth ratio ( $ald = 1.5$ , and  $2.25$ ), and stirrups 892  
reinforcement ratio ( $5\Phi6$ ,  $7.5\Phi6$ , and  $10\Phi6/m'$ ). Fourteen 893  
PVA-mortar beams were experimentally tested. Predictions 894  
of the results were carried out using a rational empirical 895  
arch-truss approach. The following conclusions were 896  
drawn from this study. 897

Failure modes of all the test beams were in shear. 898  
However, the addition of PVA had a significant effect on 899  
the crack pattern and it allowed for several vertical flexural 900  
cracks to form giving warnings prior to failure. The number 901  
and width of these cracks differ with the PVA%,  $ald$ , and 902  
stirrups. PVA-mortar beam specimens showed less but 903  
wider cracks prior to failure compared to the beam speci- 904  
mens without PVA fibres. 905

Reducing  $ald$  led to raising first crack loads and ultimate 906  
loads, improving ductility and, in turn, shear capacity 907  
without changing the mode of failure. The utmost 908  
enhancement in the performance of the test beams was 909  
achieved with PVA fibres content of 2.25% and  $ald$  equals 910  
1.5 where the enhancement of energy absorption was 365% 911  
over that in a beam without fibres. 912

PVA played the same role as the stirrups and contributed 913  
to the shear behaviour of studied beams. The contribution 914  
of PVA to ultimate shear capacity was increased with 915  
reducing the amount of shear reinforcement (stirrups). 916

Table 11 Comparison between experimental and predicted ultimate shear strength results

Group	Beam	$V_{u, exp.}$ , kN	$V_{u, Anal.}$ , kN	$V_{u, exp.}/V_{u, Anal.}$
Group A	B1	89.50	78.00	1.14
	B2	134.25	122.00	1.10
	B3	170.00	181.00	0.94
	B4	203.25	229.00	0.89
Group B	B5	95.35	80.00	1.191
	B6	148.00	124.00	1.194
	B7	232.00	195.00	1.190
	B8	264.00	251.00	1.052
Group C	B9	189.00	217.00	0.88
	B10	201.00	228.00	0.89
	B11	234.50	250.00	0.94
Group D	B12	163.30	154.00	1.060
	B13	173.10	177.00	0.97
	B14	200.00	195.00	1.026
Group E	B15	118.00	116.00	1.017
	B16	138.00	140.00	0.98
	B17	170.00	163.00	1.044
Average				1.038
Standard deviation				0.11
Coefficient of variation				10.50%

917 PVA played a significant role in beam specimens without  
918 stirrups. In addition, the PVA fibres were more effective  
919 for lower shear span to depth ratio ( $ald = 1.5$ ), where the  
920 enhancement of shear resistance was 221%.

921 For the tested PVA beams in the current study, the  
922 specimens were numerically modeled using the non-linear  
923 finite element NLFEA model using ANSYS software. The  
924 PVA fibres were simulated as smeared reinforcements in  
925 the mortar elements represented through volumetric ratio to  
926 represent the actual fibre volumes used in each beam  
927 specimen. The predicted crack pattern and load–deflection  
928 curves showed excellent agreement with the experimen-  
929 tally reported ones. The ratio of the predicted to experi-  
930 mental ultimate strength ranged between 0.91 and 1.09.

931 A proposed equation was developed in the current  
932 research which is a modification of CSA Standard [35]  
933 design equation. Good agreement was achieved between  
934 the experimental and predicted shear strength results. The  
935 ratios of [ $V_{u, exp}/V_{u, Anal.}$ ] for the studied beams ranged  
936 between 0.84 and 1.29.

937 Based on the results of the current study and for prac-  
938 tical applications, the authors recommend a combination of  
939 fly ash, silica fume and at least 1.5% PVA in the presence  
940 of minimum stirrups reinforcement (5Φ6/m) or adding  
941 2.25% PVA without stirrups to achieve adequate shear  
942 behaviour of PVA-mortar beams. This combination pre-  
943 vented sudden failure and improved the ductility as several  
944 small flexural cracks were formed prior to failure.

946 **Funding** The authors declare that they have no known competing  
947 financial interests or personal relationships that could have appeared  
948 to influence the work reported in this paper. The authors state that  
949 they did not get any funding for this research and it is self-funded.  
950

## 951 Declarations

952 **Conflict of interest** The authors declare that they have no conflict of  
953 interest.

954 **Human and animal rights** This article does not contain any studies  
955 with human participants or animals performed by any of the authors.

## 956 References

- 957 1. Pan Z, Wu C, Jianzhong L, Wang W, Jiwei L (2015) Study on  
958 mechanical properties of cost-effective polyvinyl alcohol engi-  
959 neered cementitious composites (ECC-PVA). *Construct Build*  
960 *Mater* 78:397–404
- 961 2. Li VC, Wu C, Wang SX, Ogawa A, Saito T (2002) Interface  
962 tailoring for strain-hardening polyvinyl alcohol-engineered  
963 cementitious composite (PVA-ECC). *ACI Mater J* 99(5):463–472
- 964 3. Li VC (1998) Engineered cementitious composites—tailored  
965 composites through micromechanical modeling. In: Banthia N,  
966 Bentur A, Mufti AA (eds) *Fiber reinforced concrete: present and*

- the future. Canadian Society for Civil Engineering, Montreal, pp 64–97
- 967 4. Iqbal Khan M, Fares G, Mourad S (2017) Optimized fresh and  
968 hardened properties of strain hardening cementitious composites:  
969 effect of mineral admixtures, cementitious composition, size, and  
970 type of aggregates. *J Mater Civ Eng* 29(10):04017178–1–16
- 971 5. Li, Victor C (1993) From Micromechanics to structural engi-  
972 neering - the design of cementitious composites for civil engi-  
973 neering applications. *JSCE J Struct Mech Earthq Eng JSCE J*  
974 *10(2): 37–48, <http://hdl.handle.net/2027.42/84735>.*
- 975 6. Zhang R, Matsumoto K, Niwa J, Hirata T, Ishizeki Y (2013)  
976 Experimental study on shear behaviour of PP-ECC BEAMS with  
977 different stirrups Ratios. In: *Proceedings of the Thirteenth East*  
978 *Asia-Pacific Conference on structural engineering and construction*  
979 *(EASEC-13), September 11–13, 2013, Sapporo, Japan, B-5–5., B-5–5, <http://hdl.handle.net/2115/54260>*
- 980 7. Zhu Y, Zhang Z, Yang Y, Yao Y (2014) Measurement and cor-  
981 relation of ductility and compressive strength for engineered  
982 cementitious composites (ECC) produced by binary and ternary  
983 systems of binder materials: FLY ash, slag, silica fume and  
984 cement. *Constr Build Mater* 68:192–198
- 985 8. Kanda T, Li VC (1998) Interface property and apparent strength  
986 of high-strength hydrophilic fibre in cement matrix. *J Mater Civ*  
987 *Eng* 10(1):5–13
- 988 9. Kanda T, Watanabe S (1998) Application of pseudo strain  
989 hardening cementitious composites to shear resistant structural  
990 elements”. *fracture mechanics of concrete structures*. In: *Pro-  
991 ceedings FRAMCOS-3, AEDIFICATIO Publishers, D-79104*  
992 *Freiburg, Germany, 1998, pp. 1477–1490.*
- 993 10. Alyousif A, Anil O, Sahmaran M, Lachemi M, Yildirim G,  
994 Ashour A (2016) Comparison of shear behaviour of engineered  
995 cementitious composite and normal concrete beams with differ-  
996 ent shear span lengths. *Mag Concr Res* 68(5):217–228. <https://doi.org/10.1680/jmacr.14.00336> (**Paper 1400336**)
- 997 11. Paegle I, Fischer G (2016) Phenomenological interpretation of  
998 the shear behavior of reinforced Engineered Cementitious Com-  
999 posite beams. *Cement Concr Compos* 73:213–225. <https://doi.org/10.1016/j.cemconcomp.2016.07.018>
- 1000 12. Liu H, Zhang Q, Gu C, Su H, Li VC (2017) Self-healing of micro  
1001 cracks in Engineered Cementitious Composites under sulfate and  
1002 chloride environment. *Constr Build Mater* 153(30):948–956.  
1003 <https://doi.org/10.1016/j.conbuildmat.2017.07.126>
- 1004 13. Ismail MK, Hassan AA (2019) Influence of fibre type on the shear  
1005 behaviour of engineered cementitious composite beams. *Mag*  
1006 *Concr Res*. <https://doi.org/10.1680/jmacr.19.00172>
- 1007 14. Liu Y, Zhou X, Lv C, Yang Y, Liu T (2018) Use of silica fume  
1008 and GGBS to improve frost resistance of ECC with high-volume  
1009 fly ash, Hindawi. *Adv Civ Eng*. <https://doi.org/10.1155/2018/7987589>
- 1010 15. Wang L, Zhou SH, Shi Y, Tang SW, Chen E (2017) Effect of  
1011 silica fume and PVA fibre on the abrasion resistance and volume  
1012 stability of concrete. *Compos B* 130:28–37
- 1013 16. EN 197 EN 197–2004 (2004) Cement; Composition, specifica-  
1014 tions and conformity criteria”, European standards (2004/  
1015 1–197EN)
- 1016 17. ASTM C 618 (2012) Standard Specification for coal fly ash and  
1017 raw or calcined natural Pozzolan for use in concrete. ASTM,  
1018 West Conshohocken, p 3
- 1019 18. ASTM C1240 (2015) Standard Specification for Silica Fume  
1020 Used in Cementitious Mixtures, West Conshohocken, Pennsylv-  
1021 ania; 2015
- 1022 19. Cao L (2010) Experimental study on mechanical property of  
1023 PVA-fiber reinforced cementitious composite. [Master’s thesis],  
1024 Zhengzhou, China: Henan Polytechnic University, 2010
- 1025 20. Said M, Mustafa TS, Shanour AS, Khalil MM (2020) Experi-  
1026 mental and analytical investigation of high performance concrete  
1027  
1028  
1029  
1030  
1031  
1032

- 1033 beams reinforced with hybrid bars and polyvinyl alcohol fibers. 1066  
1034 *Constr Build Mater* 259:1–22. <https://doi.org/10.1016/j.con> 1067  
1035 [buildmat.2020.120395](https://doi.org/10.1016/j.con) 1068
- 1036 21. Egyptian Standard Specifications (2002) Concrete Aggregates 1069  
1037 from natural sources”, ESS No 1109/2002 1070
- 1038 22. BS EN 934–2 2009 Edition (2009) Admixtures for concrete, 1071  
1039 mortar and grout Part 2: Concrete admixtures—definitions, 1072  
1040 requirements, conformity, marking and labelling 1073
- 1041 23. Egyptian Standard Specifications, “Steel Reinforcement Bars”, 1074  
1042 No. 262/1999 1075
- 1043 24. ECP (Egyptian Code of Practice) (2007) ECP 203-2007: design 1076  
1044 and construction for reinforced concrete structures. Ministry of 1077  
1045 Building Construction, Research Center for Housing, Building 1078  
1046 and Physical Planning, Cairo, Egypt 1079
- 1047 25. Zhou J, Qian S, Ye G, Copuroglu O, Breugel KV, Li VC (2012) 1080  
1048 Improved fibre distribution and mechanical properties of engi- 1081  
1049 neered cementitious composites by adjusting the sequence. 1082  
1050 *Cement Concr Compos* 34(3):342–348 1083
- 1051 26. Meng D, Lee CK, Zhang YX (2017) Flexural and shear beha- 1084  
1052 viours of plain and reinforced polyvinyl alcohol-engineered 1085  
1053 cementitious composite beams. *Eng Struct* 151:261–272. [https://doi://](https://doi.org/10.1016/j.engstruct.2017.08.036) 1086  
1054 [doi.org/10.1016/j.engstruct.2017.08.036](https://doi.org/10.1016/j.engstruct.2017.08.036) 1087
- 1055 27. Qudah S, Maalej M (2014) Applications of engineered cementi- 1088  
1056 tious composites (ECC) in interior beam-column connections for 1089  
1057 enhance seismic resistance. *Eng Struct* 69:235–245. [https://doi.](https://doi.org/10.1016/j.engstruct.2014.03.026) 1090  
1058 [org/10.1016/j.engstruct.2014.03.026](https://doi.org/10.1016/j.engstruct.2014.03.026) 1091
- 1059 28. Hasib M, Hossain K (2016) Shear resistance of composite beams 1092  
1060 without shear reinforcement. In: Resilient Infrastructure Confer- 1093  
1061 ence, June 1–4, 2016, pp. STR-928–1–8 1094
- 1062 29. Shimizu K, Kanakubo T, Kanda T, Nagai S (204) Shear behavior 1095  
1063 of steel reinforced ECC-PVA beams. In: 13th World Conference 1096  
1064 on Earthquake Engineering, Vancouver, B.C., Canada, August 1097  
1065 1–6, 2004, Paper No. 704 1098
30. Said M, Abd-Elazim A, Ali M, Elghazaly H, Shaaban IG (2020) 1066  
1067 Effect of elevated temperature on axially and eccentrically loaded 1068  
1069 columns containing polyvinyl alcohol (PVA) fibres. *Eng Struct.* 1070  
1071 <https://doi.org/10.1016/j.engstruct.2019.110065> 1072
31. Hossain KMA, Hasib S, Manzur T (2020) Shear behavior of 1073  
1074 novel hybrid composite beams made of self-consolidating con- 1075  
1076 crete and engineered cementitious composites. *Eng Struct* 1076  
1077 202:109856 1078
32. ANSYS–Release Version 14.5 (2012) A finite element computer 1079  
1080 software and user manual for nonlinear structural analysis. 1081  
1082 ANSYS Inc., CanonsburgA 1083
33. Shanour AS, Said M, Arafa AA, Adam A (2018) Flexural per- 1084  
1085 formance of concrete beams containing engineered cementitious 1086  
1087 composites. *Constr Build Mater* 180:23–34 1088
34. Soroushian P, Lee C-D (1989) Constitutive modeling of steel 1089  
1090 fiber reinforced concrete under direct tension and compression. 1091  
1092 Fiber reinforced cements and concrete: recent developments. In: 1093  
1094 Proceedings of an International Conference held at the University 1094  
1095 of Wales, College of Cardiff, School of Engineering, UK, Sep. 1096  
1097 18-20, 1989, pp 363–377 1098
35. CSA Standard A23.3–04 (2004) Canadian standard association 1099  
1100 (CSA). Design of concrete structures, CSA standard A23.3–04, 1100  
1101 Rexdale, Ontario. 2004. 1101
36. Beshara FB, Mustafa TS, Mahmoud AA, Khalil M (2020) Con- 1102  
1103 stitutive models for nonlinear analysis of SFRC Corbels. *J Build* 1103  
1104 *Eng* 28:1–15. <https://doi.org/10.1016/j.job.2019.101092> 1104
37. Yang E, Li VC (2010) Strain-hardening fiber cement optimiza- 1105  
1106 tion and component tailoring by means of a micromechanical 1106  
1107 model. *Constr Build Mater* 24:130–139 1107

UNCORRECTED